RFP-3387
UC-60

A CATALOG OF LOW REYNOLDS NUMBER AIRFOIL DATA FOR WIND TURBINE APPLICATIONS

February 1982

S.J. Miley

Prepared by

Department of Aerospace Engineering
Texas A&M University
College Station, Texas 77843

For

Rockwell International Corporation
Energy Systems Group
Rocky Flats Plant
Wind Systems Program
Golden, Colorado 80402-0464

Subcontract No. PFY12781-W

As Part of the

UNITED STATES DEPARTMENT OF ENERGY
WIND ENERGY TECHNOLOGY DIVISION
FEDERAL WIND ENERGY PROGRAM

Contract No. DE-AC04-76DP03533

TABLE OF CONTENTS

LIST OF SYMBOLS

SYMBOL	
c	Airfoil chord length, m
C_D	Airfoil drag coefficient
C_L	Airfoil lift coefficient
C_M	Airfoil pitching moment coefficient
D	Airfoil drag force, N
l	Characteristic body length used for Reynolds number, m
L	Airfoil lift force, N
M	Airfoil pitching moment, N-m
p	Static pressure of a fluid flow, N/m^2
x	Airfoil chordwise position
V	Flow velocity, m/s
α	Airfoil angle of attack
ρ	Density of the fluid, kg/m^3
∞	Refers to free stream flow
c/4	Refers to $\frac{1}{4}$ chord position
a.c.	Refers to airfoil aerodynamic center position

I. INTRODUCTION

Developers of small wind energy conversion systems (SWECS) which utilize conventional airfoil shapes depend upon the availability of low Reynolds number airfoil data for design and performance analyses. Existing airfoil data cover a wide range of flow conditions: low Reynolds number, high Reynolds number, incompressible, subsonic, transonic, supersonic, etc. Of this, the data which are applicable to the low Reynolds numbers of SWECS operations constitute a small portion. For reasons which will be described shortly, the available low Reynolds number data have been widely scattered, and relatively more difficult to locate, collect and verify. It is the purpose of this catalog to make these data available in one source. This catalog is the only complete collection of the best available low Reynolds number data. In addition to the presentation of the data, the catalog provides a review of airfoil theory and discusses the importance of Reynolds number, surface roughness and turbulence in airfoil performance.

In general terms, the Reynolds number is defined mathematically as,

$$R_N = \frac{(\text{velocity})\cdot(\text{density})\cdot(\text{length})}{(\text{viscosity})} \qquad (1)$$

For air at standard sea level conditions of density and viscosity, one can write

$$R_N = 69{,}000\ V\cdot l \qquad (2)$$

where V and l are given in mks units. The Reynolds number parameter is used in many different ways in accounting for flow frictional effects, and the particular flow velocity and geometric length used will vary from one application to another. For airfoil sections, the velocity is the flow velocity seen by the airfoil and the length is the airfoil chord, i.e. the distance from nose to tail of the airfoil. For a Reynolds number representative of SWECS operation, we assume l = 0.3 m and V = 40 m/s giving a value of

$$R_N \cong 830{,}000 = 8.3 \times 10^5$$

This value appears quite large. However, if we use velocity and length numbers representative of conventional propeller driven aircraft, say l - 1.5 m and V = 80 m/s, we obtain

$$R_N \cong 8{,}300{,}000 = 8.3 \times 10^6$$

SWECS operate at Reynolds numbers an order of magnitude below conventional aircraft.

Reynolds number affects airfoil lift and drag behavior. Airfoil data for one Reynolds number will not necessarily be valid for another Reynolds number. A general representation of the effects of Reynolds number on airfoil behavior is given in Figure 1.

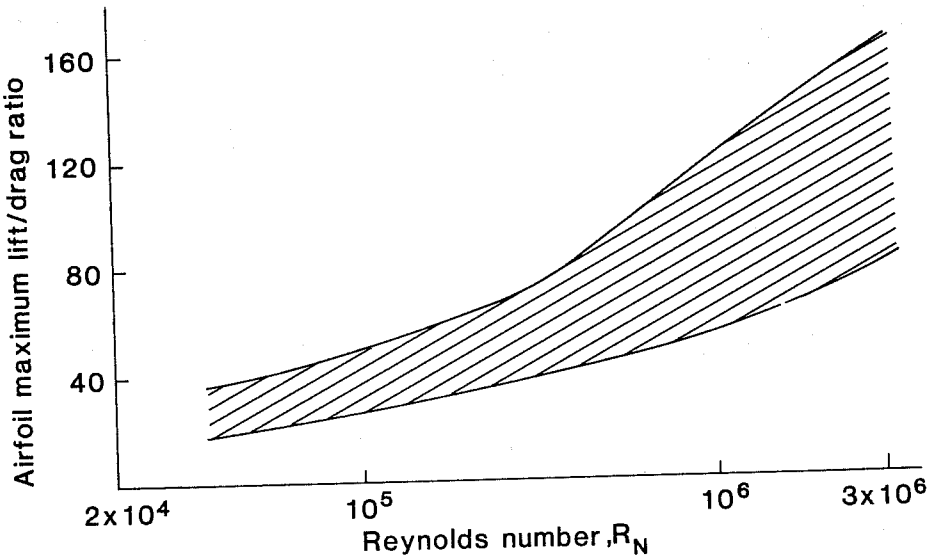

Figure 1. Effect of Reynolds number on airfoil maximum lift/drag ratio for a large number of different airfoils.

The maximum lift-to-drag ratio of an airfoil is an important performance parameter which is often used in airfoil selection. As the Reynolds number decreases, so does the lift-to-drag ratio. In fact, as the Reynolds number decreases, the maximum lift of an airfoil decreases and the minimum drag increases. The SWECS developer is, as a consequence, faced with some technical problems in airfoil selection and system aerodynamic performance evaluation.

Until recently, airfoil development has been directed solely toward aircraft applications. This is reflected by the higher Reynolds number of the vast majority of the available data. What low Reynolds number

data existed resulted from early wind tunnel testing in tunnels which were not sufficiently sized or powered to generate aircraft-range Reynolds numbers. In recent times, some effort has been expended to develop airfoils for sailplanes and flying model aircraft whose Reynolds numbers fall within the SWECS range. In order to assist the SWECS developer in airfoil selection and aerodynamic performance evaluation, an extensive survey was performed to identify and compile into a catalog all available airfoil data which is applicable to the Reynolds number operating range of SWECS. Table I lists the technical publication indices and the libraries used in the survey.

The data presented in this catalog are the best currently available to the public in terms of validity. The data are given in both tabular and graphical form. To assist the SWECS developer in the selection process, a discussion is presented, in elementary terms, of the various factors that influence airfoil performance. These include Reynolds number, surface roughness and flow turbulence.

TABLE I
INFORMATION SOURCES USED

Technical Report Indicies:	
National Advisory Committee for Aeronautics (NACA)	1915-1958
National Aeronautics and Space Administration, Scientific and Technical Reports (NASA STAR)	1958-1980
National Technical Information Service (NTIS)	1946-1980
United States Government Research and Development Reports	1960-1980
Great Britain Aeronautical Research Council, Reports & Memoranda	1910-1980
Technical Publication Indicies:	
Institute of the Aeronautical Sciences	1947-1958
American Institute of Aeronautics and Astronautics, International Aerospace Abstracts	1960-1980
Engineering Index	1920-1980
Dissertation Abstracts	1910-1980
Libraries:	
NASA Langley Research Center	
NASA Ames Research Center	
Library of Congress	
National Air and Space Museum	
National Archives	
NASA Archives	
Texas A&M University	
Georgia Tech	
MIT	

II. AIRFOIL CHARACTERISTICS

1. Airfoil Geometric Description

The importance of the geometric characteristics of the airfoil shape has varied over the years. Always of prime concern is the ability to reproduce the desired airfoil shape from tabulated data. In addition, the empirical approach to airfoil development, which was used through the first half of the 20th century, resulted in the creation of a number of geometric shape parameters to allow correlation with test results. With the present airfoil design state-of-the-art (which is analytically based) some of these parameters have become obsolete. Figures 2-4 present a summary of the important geometric parameters and indicate which are obsolete. In Figure 2, the parameters which are used to develop the airfoil shape are shown.

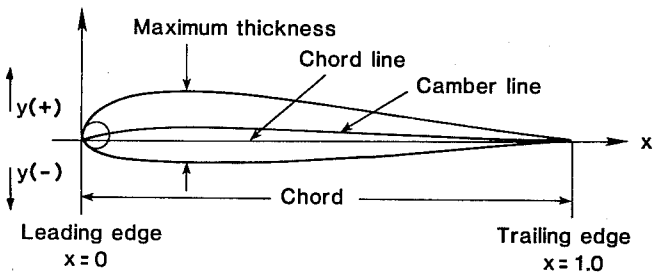

Figure 2. Important airfoil geometric quantities.

The chord line is the reference line of the airfoil, and is the line connecting the most extreme points at the leading and trailing edges. The chord is the reference length of the airfoil and is measured along the chord line. The value of the chord dimension is the distance between the extreme leading and trailing edge points. All other dimensions are referenced to the chord. Most NACA airfoils specify a leading edge radius to connect the upper and lower surface contours. The radius is struck from a line, intersecting the chord line at the leading edge, and which may be at an angle to the chord line. If so, then the angle is specified in terms of the slope of this line measured relative to the chord line. This is illustrated in Figure 3.

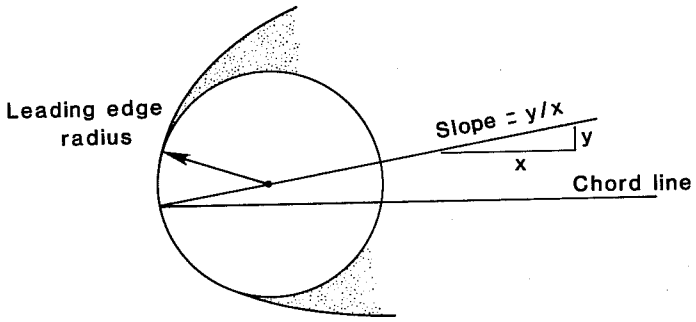

Figure 3. Development of leading edge radius.

The airfoil contour is specified by two sets of X-Y coordinates, one for the upper surface and one for the lower surface. In many cases, the same X coordinate is used for both the upper and lower surface Y coordinates. The numerical values of the coordinates are normally presented in one of two formats, both referenced to the airfoil chord. In one format, all values are divided by the chord, with X having the value 0.0 at the leading edge and 1.0 at the trailing edge. The coordinate data presented in this catalog are in this format. In the other format, the values are given in terms of percent of chord with X having the value 0 at the leading edge and 100 at the trailing edge. In both formats, the true airfoil shape dimensions are obtained by multiplying the coordinates by the desired chord dimension. Other airfoil geometric quantities shown in Figure 2 which are still in use are the maximum thickness and the camber line. Maximum thickness is normally specified in terms of percent chord. The camber line is the line which is equidistant from the upper and lower surfaces. It represents the amount of curvature incorporated in the overall airfoil shape. In the empirical airfoil development era, the amount of camber and shape of the camber line were of major importance. Now, camber is used mainly in a qualitative sense to indicate the general lifting behavior of the airfoil, i.e., a high cambered airfoil will generate more lift than a low cambered airfoil.

Geometric parameters which are now considered obsolete are indicated in Figure 4.

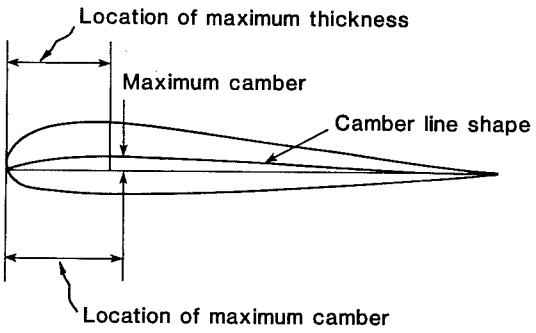

Figure 4. Airfoil geometric quantities no longer in use.

These include maximum camber, location of maximum camber, location of maximum thickness, and shape of the camber line. These quantities were important in the empirical airfoil design era, which led to the NACA four-digit, five-digit, and six-digit airfoils, but are no longer of any use in present design methods.

A geometric characteristic which is of little importance aerodynamically, but may be of concern from a structural point of view, is the airfoil thickness distribution. This is the variation in thickness along the X coordinate. Figure 5 shows two airfoils of the same thickness but different thickness distributions.

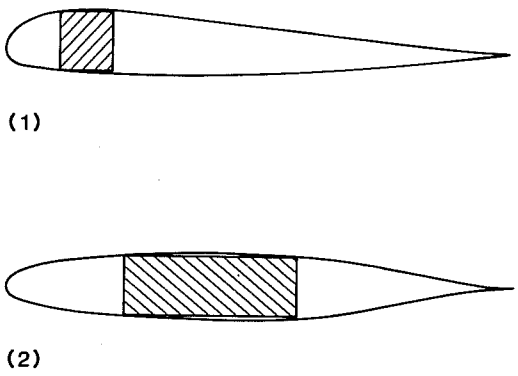

Figure 5. Airfoils of the same thickness but different thickness distributions.

Box beam spars of the same depth are shown embedded in each. This thickness distribution of the number (2) airfoil allows the use of a more

effective box beam structure with greater stiffness-to-weight capability. In the past, the thickness distribution was also used in the creation of airfoil section families. An airfoil family is a series of shapes having the same thickness distribution, but varying in one or more of the other geometric parameters in a systematic manner. A particular airfoil shape is obtained by combining a thickness distribution with a camber line as illustrated in Figure 6.

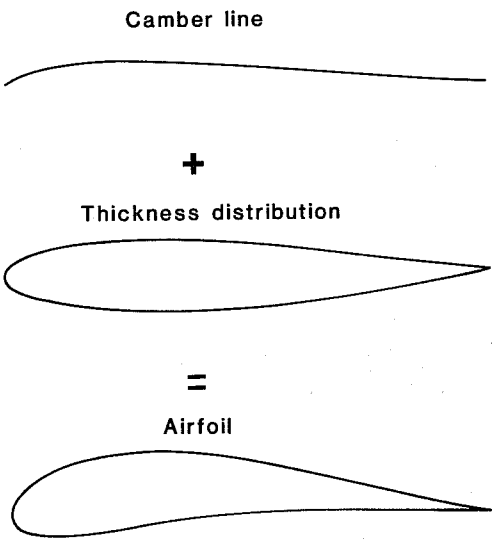

Figure 6. Geometric development of an airfoil from a camber line and a thickness distribution.

The system of designating airfoils varies from source to source. The most consistent are the airfoils developed by NACA. The NACA airfoils come in three series, four-digit, five-digit, and six-digit. Examples of these are: NACA 4412, NACA 23015, and NACA 63_1-412. The combination of digits in the designation contain coded information concerning theoretical lift characteristics and geometry characteristics of the respective airfoil. The coding varies for each series, but the last two digits always give the maximum thickness in percent chord. The relative aerodynamic performance of each series increases in the order listed. The five-digit series is superior to the four-digit and the six-digit is superior to the five-digit. Respective airfoil performance characteristics are included in the coding for the NACA five-digit and six-digit series; however, these are generally not realized in practice at SWECS Reynold's numbers ($R_N < 3 \times 10^6$), and are not discussed here. Additional information on the NACA airfoils can be found in Reference 1. The other two major series which appear in the catalog are designated differently. The Gottingen-Go series are designated in the order of development. There is no code involved in the sequence of digits. The Wortmann FX-series designations appear to have changed over a period of time. The last three digits normally indicate the maximum thickness in percent chord to the nearest one tenth. The first two digits seem to indicate the year of development. For example, the FX 61-184 would be 18.4 percent thick and would have been developed in 1961.

2. Airfoil Forces and Moments

An airfoil is a geometric shape designed to generate a mechanical force as a result of relative motion between it and a fluid. The term fluid here means that this physical effect occurs equally for both liquids (i.e., water) and gases (i.e., air). Applications to water result in the designation airfoil being changed to hydrofoil. The term relative motion means that the effect occurs regardless of whether the airfoil is stationary and the fluid is moving; the fluid is stationary and the airfoil is moving; or both are moving. The force generated by the airfoil is often called lift because most applications are to aircraft wings. However, different terms may be used for other applications. For example, the vertical stabilizer of an aircraft is an airfoil whose lift force is horizontal rather than vertical. The term lift here may be replaced by side force or normal force. While the lift force is of prime concern, an additional force, the drag force, and a torquing force or pitching moment are also generated by the airfoil. An airfoil and its associated forces are shown in Figure 7.

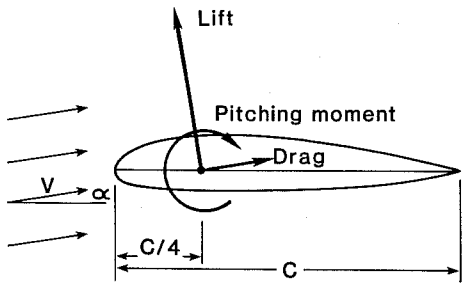

Figure 7. Aerodynamic forces developed by the airfoil: lift, drag and pitching moment.

The indicated force directions are considered positive. The resolved point of application of these forces is at the one-quarter chord point on the airfoil.

The lift force and pitching moment are generated by the variation of the fluid pressure about the airfoil. The pressure, in turn, is related to the fluid velocity about the airfoil through Bernoulli's equation

$$P + \tfrac{1}{2} \rho V^2 = \text{const.} \qquad (3)$$

The term $(1/2\ \rho V^2)$ is called dynamic pressure, and is the component of the pressure acting on a body due to the fluid velocity. The Bernoulli equation is a fundamental fluid motion relationship which, among other

things, states that regions in the flow where the fluid velocity is high correspond to regions where the fluid pressure is low, and conversely, regions of low velocity correspond to regions of high pressure. Consequently, the fluid velocity and pressure about the airfoil are interrelated, and one can consider that the lift and pitching moment forces result from variations in velocity about the airfoil as well as pressure. The approach that is used in present day airfoil analyses and design is to work with the velocity variation about the airfoil and convert to pressure using the Bernoulli equation when the resulting force magnitudes are required.

The drag force results from the frictional behavior of fluid flow. This behavior, which is relatively complex in practice, is discussed in some detail in Section III. For the present, the drag force results from a combination of friction forces acting on the airfoil surface and pressure forces. The relative contributions of friction and pressure to the drag force change with the flow angle to the airfoil.

Consideration of the various physical quantities which may be involved in the generation of the aerodynamic forces of lift, drag and pitching moment lead to the following standardized relations:

Lift	$L = C_L(\frac{1}{2}\rho V^2)A$	(4)
Drag	$D = C_D(\frac{1}{2}\rho V^2)A$	(5)
Pitching Moment	$M = C_M(\frac{1}{2}\rho V^2)cA$	(6)

All three have in common the dynamic pressure term from Bernoulli's equation as well as the planform area of the wing. In addition, the pitching moment relation includes the airfoil chord length c. The planform area is the product of the chord length to the lateral span of the actual wing or blade using the airfoil. This is not the true surface area, but the projected or outline area when viewed from above or below. The respective coefficients C_L, C_D and C_M represent the performance characteristics of the particular airfoil. Their values are controlled by the airfoil shape and by other physical quantities associated with the fluid flow. Chief among these is the angle of attack, which is the angle between the direction of flow and the airfoil chord line. The coefficients are also affected by the frictional behavior of the flow, which is represented by the Reynolds number parameter. The Reynolds number effects will be discussed in Section III.

As shown in Figure 7, angle of attack is the angle of the airfoil chord line relative to the direction of the flow. The lift force acts perpendicular to the flow direction and the drag force acts parallel to the flow direction. Thus, the directions of the lift and drag forces

relative to the airfoil change with angle of attack. Sometimes, lift and drag are combined into two other force components, normal and chord force, which are always perpendicular and parallel respectively to the airfoil chord line. Also, the pitching moment is often taken about another reference point called the aerodynamic center whose location can vary. Strictly, the pitching moment terms M and C_M should include additional subscripts denoting the reference point about which they are applied, i.e., $M_{c/4}$, $C_{Mc/4}$, or $M_{a.c.}$, $C_{Ma.c.}$. This will not be done here in order to maintain clarity. All references to pitching moment in this report refer to the one-quarter chord length location, i.e. $C_M = C_{Mc/4}$.

The performance characteristic coefficients for a particular airfoil are most often presented in graphical form as shown in Figure 8.

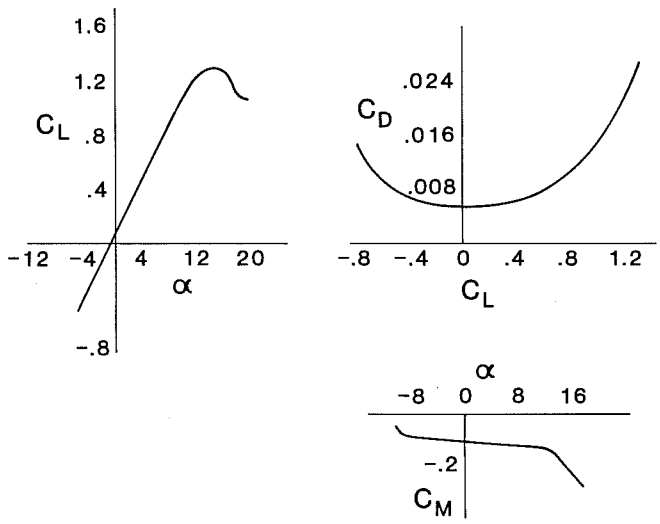

Figure 8. Conventional graphical presentation of airfoil characteristics.

The lift and pitching moment coefficients are plotted as functions of the angle of attack, while the drag coefficient is plotted as a function of lift coefficient. Some variations of this format occur, mainly in regard to the plotting of the drag and pitching moment data. To retain consistency with the tabular data, all performance coefficients in this report are plotted as a function of angle of attack.

The coefficient behavior shown in Figure 8 is typical. There is a range of angle of attack where the lift coefficient varies linearly. At some point, a maximum value of lift coefficient is reached where a further increase in angle of attack causes a decrease (sometimes a very rapid decrease) in lift. This is referred to as stall and the reasons for it are

discussed later. There is a region of lift coefficient (and corresponding angle of attack) where the drag coefficient has its lowest values. Outside this range, it increases, again sometimes rapidly. This increase is related to the stall which also causes the loss in lift. The pitching moment coefficient is almost always negative and tends to go more negative as the angle of attack increases. Rapid changes occur in this coefficient also at stall. A negative pitching moment coefficient corresponds to a nose down torque force acting on the airfoil. A positive pitching moment corresponds to a nose up torque force as shown in Figure 7.

III. AIRFOIL AERODYNAMICS

1. Boundary Layer Behavior

When there is relative motion between a solid body and a fluid, the fluid flow about the body can be divided into two regions: one where frictional effects are negligible and the other where frictional effects are significant. The significant friction region is in the flow immediately next to the body, and is referred to as the boundary layer. This is the case for both liquids and gases. The extent of the flow region away from the body which is included in the boundary layer, i.e., the thickness of the boundary layer, varies from a fraction of an inch to inches for airflow. For large ships in water, the boundary layer thickness is on the order of several feet.

The flow within the boundary layer is relatively complex. The flow velocity varies from zero at the surface of the body to the value of the friction-free flow outside of the boundary layer. The flow in the boundary layer exists in one of two states: laminar or turbulent. Laminar flow is smooth and uniform and resembles the friction-free flow away from the body. Turbulent flow is rough and disorganized. Laminar flow destabilizes and changes to turbulent flow when certain physical limiting conditions within the boundary layer flow are exceeded. The process of this change is called transition. The basic character of the boundary layer and its laminar, transition and turbulent regions is illustrated in Figure 9.

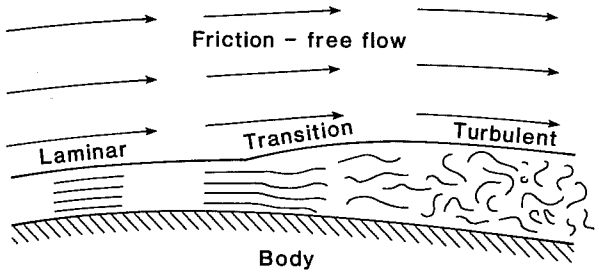

Figure 9. Boundary layer flow adjacent to a solid body in a fluid flow.

The dividing line between boundary layer flow and friction-free flow, i.e. the boundary layer thickness, is arbitrarily taken to be the point where the boundary layer flow velocity is ninety-nine percent of the friction-free flow velocity.

The friction part of the drag force is generated in the boundary layer. The magnitude of the friction force depends on the character of the boundary layer, and on the Reynolds number. Laminar boundary layers generate relatively low frictional forces whereas turbulent boundary layers result in relatively large friction forces. This is why laminar flow is desired over as much of a body as practical as a means of reducing drag. Older airfoils may have a laminar boundary layer over the first twenty percent of their surface, whereas more recent "low drag" laminar airfoils can have a laminar boundary layer over as much as seventy percent of their surface. For both laminar and turbulent flows, the friction force varies with the reciprocal of the Reynolds number. As will be seen with the airfoil data, as the Reynolds number decreases, the drag force coefficient increases.

Both laminar and turbulent boundary layers are affected by the pressure gradient of the flow. This is the variation of the pressure in the direction of the flow. A favorable pressure gradient is one where the pressure decreases in the direction of the flow, an adverse gradient is one where the pressure increases in the direction of the flow. Referring to the Bernoulli equation (Equation 3), the flow velocity accelerates with a favorable pressure gradient and decelerates with an adverse pressure gradient. If we write Equation (3) for two adjacent points in the flow and take the difference, we obtain

$$(p_1 - p_2) = -\tfrac{1}{2}\rho\,(V_1^2 - V_2^2). \qquad (7)$$

If the pressure increases from point 1 to point 2 ($p_1 < p_2$), then the velocity must decrease from point 1 to point 2 ($V_1 > V_2$) and vice versa. Because of frictional forces at work, boundary layer flows lack the energy to move against an adverse (increasing) pressure gradient over an extended length. What happens is illustrated in Figure 10. The variation in velocity across the boundary layer is shown at points along the flow path for a favorable (decreasing) pressure gradient in the upper figure, and an adverse (increasing) pressure gradient in the lower figure. The adverse pressure gradient, working against the flow, eventually forces the flow near the body surface to reverse direction and move toward the decreasing pressure. In most situations, once flow reversal is reached in the boundary layer, the external flow pattern breaks down, and the flow separates from the body, forming a large turbulent wake. This is illustrated in Figure 11 for an airfoil.

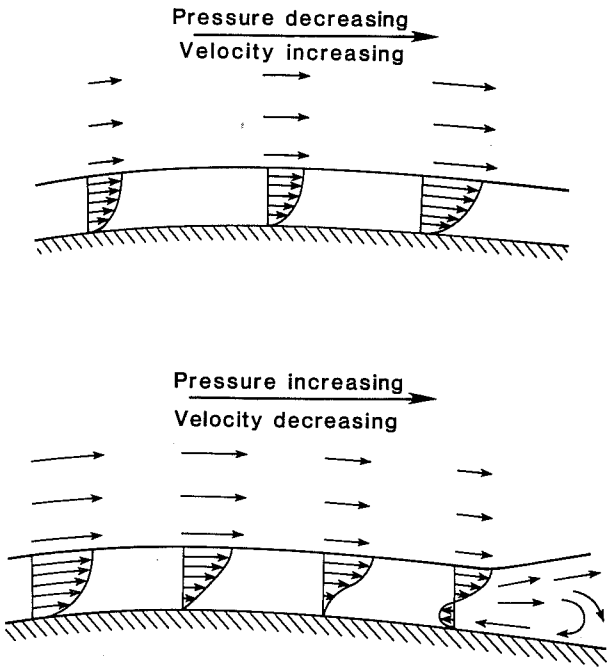

Figure 10. Effects of favorable (decreasing) and adverse (increasing) pressure gradients on the boundary layer.

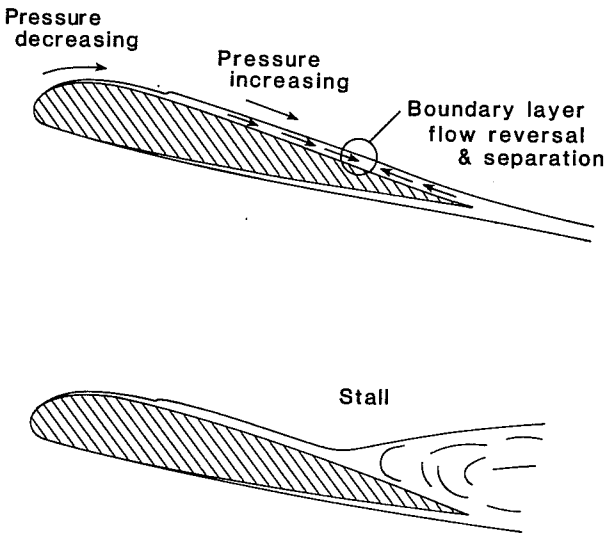

Figure 11. Boundary layer flow separation and subsequent stall.

This separation is called stall, and may involve part or all of either the upper or lower surface of the airfoil. The change in flow pressure which accompanies separation causes a decrease in lift and an increase in drag. The pressure component of drag comes from flow separation. The effect of pressure on fluid flow is analogous to the effect of the ground slope on water flowing from a hose. If the hose is pointed downhill, the water flows smoothly and accelerates as it moves downhill. If the hose is pointed uphill, the water flows uphill with a decreasing velocity. A point is reached where the flow velocity decelerates to zero then reverses direction and begins to flow downhill. Water likes to flow downhill; it does not like to flow uphill. The boundary layer likes to flow with a decreasing pressure; it does not like to flow against an increasing pressure.

Comparatively, the laminar boundary layer is a relatively fragile flow. It can withstand only negligible adverse pressure gradients without separation. It is susceptible to destabilization and transition to turbulent flow. The stability of the laminar boundary layer is affected by both the pressure gradient and Reynolds number. Low Reynolds numbers and favorable pressure gradients increase stability. High Reynolds numbers and adverse pressure gradients reduce stability or destabilize. When subjected to an adverse pressure gradient, the laminar boundary layer may react in one of three ways. It may separate and produce stall, it may separate and reattach shortly thereafter as a turbulent boundary layer, or it may destabilize and become turbulent. This is illustrated in Figure 12.

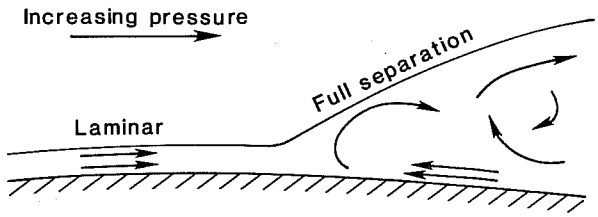

(a) Low Reynolds numbers: full separation and stall

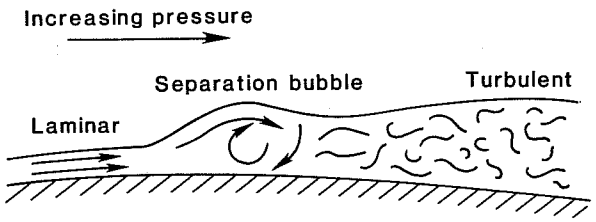

(b) Medium Reynolds numbers: separation and reattachment as turbulent.

Figure 12. Reynolds number effects on laminar boundary layer in an adverse pressure gradient.

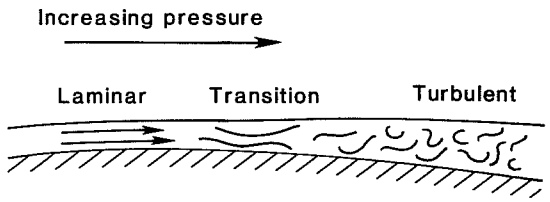

(c) High Reynolds numbers: transition to turbulent.

Figure 12. Concluded

The course taken is a complicated function of the state of the laminar boundary layer, the strength of the pressure gradient and the Reynolds number. In general terms, at low Reynolds numbers, the laminar boundary layer will tend to separate and stall (Figure 12(a)). At medium Reynolds numbers, it will tend to separate and reattach as turbulent (Figure 12 (b)). At high Reynolds numbers, it will tend to destabilize and go turbulent (Figure 12(c)). The quantitative divisions between high, medium and low Reynolds numbers have never been specifically established, but the author believes that a consensus would be;

high	$R_N > 3 \times 10^6$
medium	$5 \times 10^5 < R_N < 3 \times 10^6$
low	$R_N < 5 \times 10^5$

2. Boundary Layer Influence on Airfoil Characteristics

An airfoil generates lift by creating a difference in pressure between the upper and lower surfaces. If the direction of lift is upward, then the average pressure on the lower surface will be greater than the average pressure on the upper surface. Lift can then be produced by generating a low (suction) pressure on the upper surface, or a high pressure on the lower surface, or a combination of both. In terms of the flow velocity, this means accelerating the velocity over the upper surface and/or decelerating the velocity over the lower surface.

The variation of the flow velocity about an airfoil is a function of the airfoil shape and angle of attack. Figure 13 gives the velocity distributions over the upper and lower surfaces of a representative airfoil at four different angles of attack.

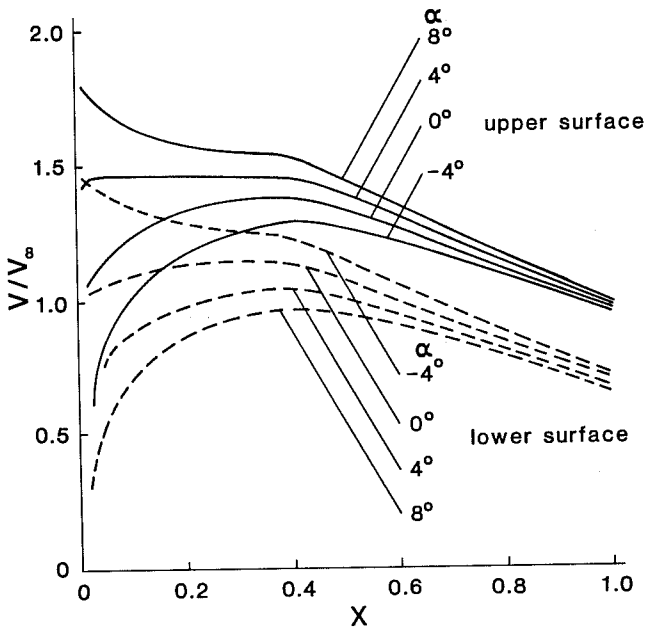

Figure 13. Typical velocity distribution about an airfoil for different angles of attack.

In studying the flow about an airfoil, the velocity of the external flow distant from the airfoil, called the free stream velocity (V_∞), is used as a reference. The actual velocity about the airfoil is analyzed and described in terms of the ratio of the airfoil velocity to the free stream velocity. This is consistent with basic airfoil behavior in that the particular performance characteristics of lift and pitching moment coefficient depend only on the relative change in velocity over the airfoil and not on the absolute value. As the angle of attack increases, the velocity over the upper surface also increases, accelerating most rapidly at the leading edge. The velocity over the lower surface decreases. The result in terms of flow pressure is that pressure decreases on the upper surface and increases on the lower surface causing lift to increase with angle of attack. As angle of attack decreases, the velocity and pressure behavior reverses itself with respect to the upper and lower surfaces. On the lower surface, velocity increases, pressure decreases, etc. The shapes of the velocity distributions on the upper and lower surface also determine the pitching moment. If the pressure difference is greater toward the trailing edge, a negative (nose-down) pitching moment will result.

Both the upper and lower surface velocity distributions in Figure 13 have adverse gradients (increasing pressure) on the rear part of the airfoil. The strength of the adverse gradients increases on the upper surface with increasing angle of attack, and increases on the lower surface with decreasing angle of attack. Considering the response of the boundary layer to adverse pressure gradients, separation and stall will occur eventually on the upper surface as the angle of attack increases, and on the lower surface as the angle of attack decreases. Also, since the laminar boundary layer is relatively weak and cannot withstand much of an adverse pressure gradient, transition to turbulent flow must occur before the major adverse gradients are encountered, otherwise a definite laminar separation and stall will result. In short, the airfoil operates as an efficient lift-producing device only as long as the associated pressure distributions can be supported by the boundary layer. The decrease in lift and increase in drag are caused by increased boundary layer separation as the angle of attack increases in both the positive and negative directions. Separation and stall occur on the upper surface as the angle of attack increases, and on the lower surface as the angle of attack decreases. This is why the drag coefficient curve increases at either end relative to lift coefficient (or angle of attack) as shown in Figure 8.

3. Effects of Reynolds Number, Roughness and Turbulence

The boundary layer of the flow about the airfoil exerts a negative influence. It works against the development of lift. The desired lift is obtained only as long as the boundary layer can withstand the lift producing pressure gradients about the airfoil. Once boundary layer separation begins, loss of lift results and the loss increases with the extent of separation. The boundary layer also produces drag through both friction forces and pressure forces when separation occurs. Reynolds number, surface roughness and turbulence all affect the boundary layer, and consequently the lift and drag behavior of the airfoil. While representing no direct effect such as roughness, the Reynolds number serves as an indicator of certain boundary layer characteristics and tendencies. Of concern are the point at which transition to turbulence occurs and the strength of the turbulent boundary layer. At high Reynolds numbers, the laminar boundary layer is less stable and transition to a turbulent boundary layer occurs sooner. The turbulent boundary layer is strong and is able to withstand large adverse pressure gradients before separating. At low Reynolds numbers, the laminar boundary layer is more stable and resistant to transition. The turbulent boundary layer is weak, and is able to tolerate only mild adverse pressure gradients. In order for an airfoil to generate lift, there ultimately must be at least one adverse pressure gradient on either the upper or lower surface. This is illustrated in Figure 14.

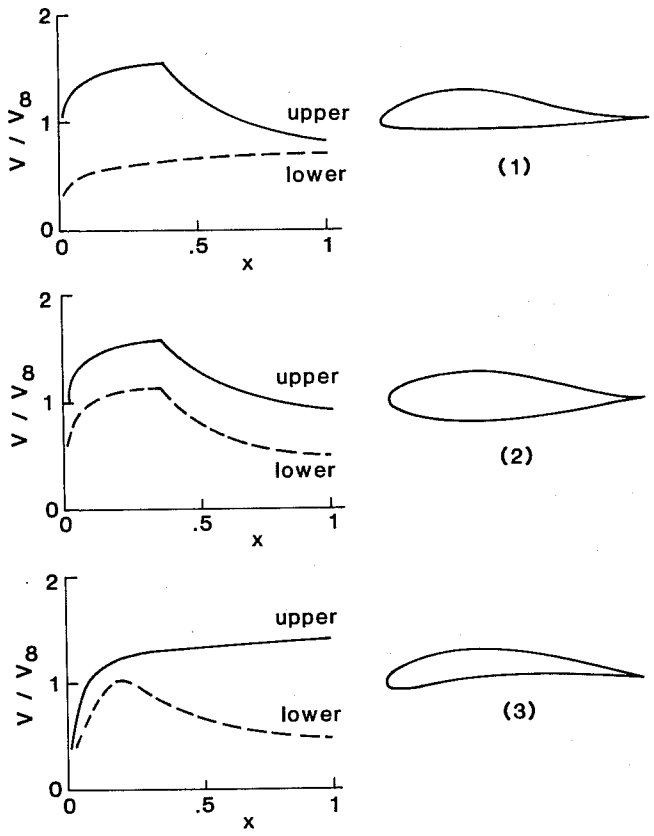

Figure 14. Development of lift through different combinations of velocity (pressure) distributions and corresponding airfoil shapes.

Airfoil (1) generates lift through low pressure on the upper surface and requires a strong adverse pressure gradient so that the corresponding high flow velocity on the upper surface can be slowed back to its free stream value at the trailing edge. Airfoil (2) utilizes a combination of low pressure on the upper surface and high pressure on the lower surface. The adverse pressure gradient on the upper surface is as strong as airfoil (1), the adverse gradient on the lower surface is more moderate. Airfoil (2) is representative of the majority of airfoils in existence, due to its suitability for aircraft applications. Airfoil (3) produces lift from high pressure on the lower surface. The adverse gradient here is the most moderate of the three. As the Reynolds number decreases, the strength of the turbulent boundary layer also decreases and the tendency for the

boundary layer to remain laminar increases. A low critical Reynolds number is ultimately reached where the boundary layer on the airfoil is totally laminar. Therefore, as the Reynolds number decreases, the boundary layer on the airfoil is less able to tolerate the adverse pressure gradients associated with the generation of lift. For a given airfoil, the maximum value of lift coefficient decrease and stall occurs sooner. Airfoils (1) and (2) are more affected by this because they utilize larger adverse pressure gradients than airfoil (3). Some airfoil (3) sections can produce moderate lift with a totally laminar boundary layer. This is why type (3) airfoils are used extensively for flying model aircraft and small lowspeed fans. The essential fact here is that a turbulent boundary layer is necessary for useful lift, and that the amount of lift possible increases with Reynolds number up to some practical limit. There is a paradox at work here in regard to airfoil utilization for high and for low Reynolds numbers. At high Reynolds numbers typical of aircraft applications, the existence of the necessary turbulent boundary layer is taken for granted and one generally works at promoting laminar flow to reduce drag. The reverse is true at low Reynolds numbers. Here one may have to work at promoting a turbulent boundary layer to achieve the desired lift. A more detailed discussion of the effects of low Reynolds numbers on airfoil performance and design can be found in Reference (2).

Surface roughness reduces the effectiveness of the airfoil. By roughness, we mean any protuberances or scratches on the airfoil's surface which can be felt by touch. The extent to which roughness affects airfoil performance is dependent on the nature of the roughness, its size relative to the boundary layer thickness, the Reynolds number and the airfoil type. Roughness destabilizes the laminar boundary layer and weakens the turbulent boundary layer in regard to adverse pressure gradients. The corresponding effects on airfoil, lift and drag depend on the particular types of pressure distributions developed by the airfoil. Boundary layer condition is more critical for airfoils which utilize low pressure on the upper surface for lift as in the case of types (1) and (2) in Figure 14. Roughness here causes noticeable reductions in maximum lift coefficient and increases minimum drag coefficient. The so-called laminar airfoils are particularly sensitive to roughness because the improved airfoil performance is obtained by tightly controlling the boundary layer behavior. Any deviations of the boundary layer from its intended behavior, such as that due to roughness, can result in significant deteriorations in performance. Reference (1) reports this behavior for the NACA six-digit series laminar airfoils in comparison with older, lower performance NACA four-digit series and five-digit series airfoils. When a smooth, high quality surface is used, the laminar series are superior. However, with surface roughness the laminar series may be inferior. The type (3) airfoils are less sensitive to roughness because the behavior of the boundary layer is less critical for the realization of the lift producing pressure distributions. Drag increases still result as with the types (1) and (2), but loss of lift is generally less.

The effects of roughness increase with increasing Reynolds numbers. This is due, in part, to the thickness of the boundary layer varying inversely with Reynolds number. At low Reynolds number, the boundary layer is relatively thick. Since the physical size of normally encountered roughness, i.e. dirt, scratches, bugs, etc., remains the same, its size relative to the boundary layer thickness increases with Reynolds number. Figure 15 shows the influence of Reynolds numbers on roughness effects for the Go 769 airfoil as reported in Reference (3).

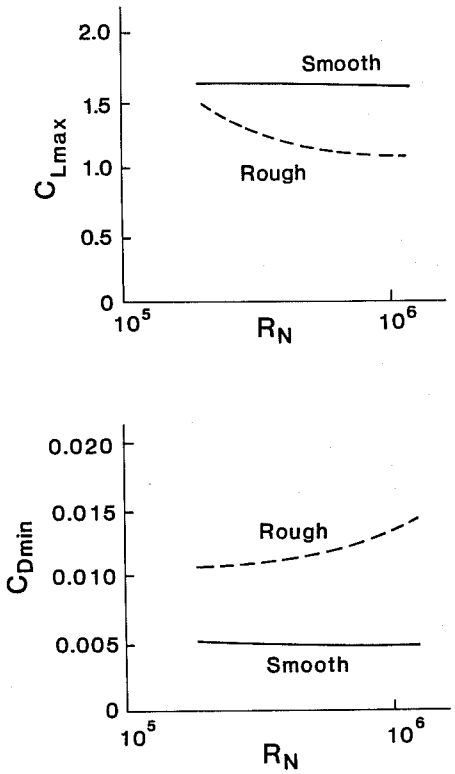

Figure 15. Influence of Reynolds number on surface roughness effects for the Go 769 airfoil.

The roughness used in the test was sand grains 0.2 mm to 0.3 mm in diameter. As the Reynolds number increases, the boundary layer thickness decreases relative to the roughness particle size, and the roughness has correspondingly more effect.

Whereas roughness is encountered under operational conditions, free stream turbulence is encountered mainly in wind tunnel tests. Up to this point, the discussion of turbulence has been restricted to that within the boundary layer. Turbulence can also exist in the external friction-free flow. Free stream turbulence readily exists in any internal flow system such as a wind tunnel. It is created by the drive fan and by bends and

corners in the flow duct. Airfoil data obtained from wind tunnels with high turbulence levels (>0.4% V_∞) are not truly representative of the respective airfoil behavior in free air. The chief effect of turbulence is to destabilize the laminar boundary layer and force transition sooner than it would otherwise occur. The turbulent boundary layer is thus more extensive and as a consequence, the frictional component of drag is greater. A comparison of test data for the same airfoils shows the minimum drag coefficient may double in value as a result of turbulence. Laminar airfoils, which rely on extensive laminar flow, are much more sensitive than other types. At low Reynolds numbers, free stream turbulence can increase the maximum lift coefficient beyond what it would be in smooth flow. This is because it promotes the turbulent boundary layer which is necessary for the increased lift. Consequently, airfoil data at low Reynolds number from high turbulence wind tunnels may be optimistic in maximum lift coefficient for operation in free air.

As SWECS operate in the atmosphere (which is certainly a turbulent flow), the question arises as to how this affects airfoil behavior. The scale of turbulence is the deciding factor here. The airfoil boundary layer is sensitive only to turbulent fluctuations on the order of the size of the boundary layer thickness itself. The frequency of these fluctuations is within the audio range. The scale of atmospheric turbulence is too large to have any direct effect on the boundary layer. It may have an indirect effect by causing a fluctuation in the airfoil angle of attack, and consequently, the airfoil pressure distribution. If we consider an aircraft flying through atmospheric turbulence, the turbulence scale is on the order of the size of the airplane, and it responds accordingly by bouncing around. The scale is too large to be seen by the boundary layer as other than a variation in the wing angle of attack.

IV. INTERPRETATION AND UTILIZATION OF AIRFOIL DATA

1. Methods of Testing

Airfoil data are obtained almost exclusively from wind tunnel tests. Some data are collected from actual aircraft wings or rotor blades under operational conditions, but these are not necessarily considered as true airfoil data.

There are two basic kinds of wind tunnel configurations in use: open-return and closed-return. These are illustrated in Figure 16.

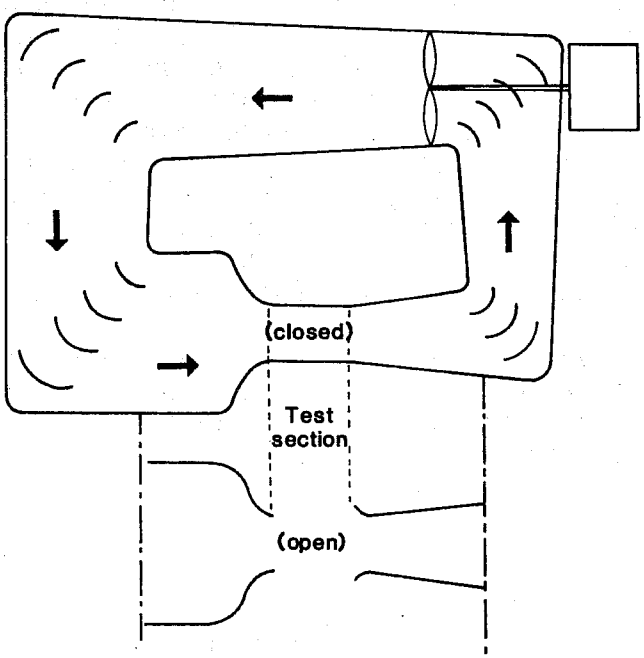

(a) Closed return with open or closed test section.

Figure 16. Basic wind tunnel configurations.

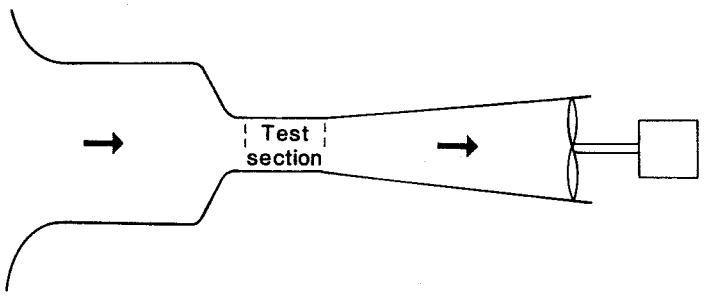

(b) Open return.

Figure 16. Concluded

The closed-return tunnel is more efficient and is capable of higher test speeds than the open-return. However, the open-return tunnel uses external air rather than recycled flow, and can produce test flows with lower turbulence levels. The open-return tunnel is preferable for low-speed airfoil testing because of the quality of its flow. As indicated in Figure 16, the open-return tunnel has a closed test section, but the closed-return tunnel may have either an open or closed test section depending upon the particular design. Data from a closed test section have to be corrected for the effects of the test section walls on the flow about the test model. Early wind tunnels utilized open test sections to avoid this. The open test section design is inherently speed limited however, and except for special V/STOL aircraft tests, most all wind tunnel testing today is performed with closed test sections.

Airfoil data have been obtained using one of two test modes: two-dimensional testing or three-dimensional testing. In three-dimensional testing, a wing is constructed using the test airfoil and placed in the test section as shown in Figure 17(a).

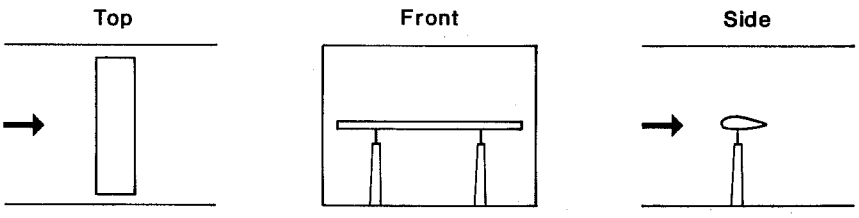

(a) Three-Dimensional model.

Figure 17. Airfoil test model configurations.

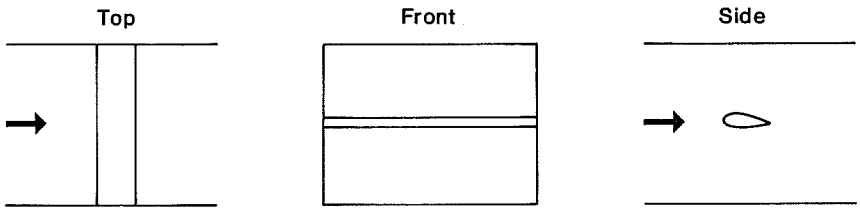

(b) Two-Dimensional model.

Figure 17. Concluded

The wing angle of attack is varied, and the lift, drag and pitching moment forces are measured by a force-balance system. The data are reduced to coefficient form using the wing area and the velocity values. Most of the early airfoil data, including the Gottingen data in this catalog were obtained this way. This mode of testing poses problems in accounting for the effects of the three-dimensional flow about the wing tips, particularly at high angles of attack where flow separation and stall begin to appear. Accounting for the effects of the test section walls is also more difficult here.

In the two dimensional mode of testing, the wing extends across the test section and intersects the walls (Figure 17(b)). There are no wing tips to create a three-dimensional flow. The flow everywhere is two-dimensional. Corrections for wall effects are relatively easier to arrive at. Airfoil lift and pitching moment are determined from pressure measurements made on the test model or from the test section walls parallel to the model. Drag is determined by measuring the boundary layer wake downstream of the model. The flow in this region has been slowed by the friction forces acting on the wing. In essence, drag comes from slowing the flow velocity, and can be determined by measuring the extent to which the flow velocity has been reduced. Two-dimensional test data is more reliable than three-dimensional test data, due mainly to the uncertainties in three-dimensional data introduced by the flow about the wing tips, particularly at high angles of attack.

2. Correlations Between Different Tests

The data in this catalog came from a number of different wind tunnels. These are described in Table II. Of these, only the Stuttgart and NASA LTPT tunnels are still active in airfoil testing. Data from the MVA/AVA Gottingen and NACA VDT tunnels are three-dimensional tests whose results have been corrected to equivalent two-dimensional results. The NACA LTT, NASA LTPT

TABLE II

DESCRIPTION OF WIND TUNNELS SUPPLYING AIRFOIL DATA

Tunnel	Type	Test Section	Velocity	Turbulence	Designation
Mechanische Versuchsanstalt Gottingen 2 m x 2 m	Closed Return	2 m x 2 m (Closed)	10 m/s	0.9%	MVA 2 m x 2 m
Aerodynamische Versuchsanstalt Gottingen 2.25 m	Closed Return	2.25 m Circular (Open)	50 m/s	0.24%	AVA 2.25 m
Aerodynamische Versuchsanstalt Gottingen 4 m x 5.4 m	Closed Return	4 m x 5.4 m elliptical (Closed)	104 m/s	0.3%	AVA 4 m x 5.4 m
National Advisory Committee for Aeronautics Variable Density Tunnel	Closed Return	1.5 m Circular (Closed)	22 m/s	2.00%	NACA VDT
National Advisory Committee for Aeronautics Low-Turbulence Tunnel	Closed Return	0.9 m x 2.29 m (Closed)	70 m/s	0.03%	NACA LTT
National Aeronautics and Space Administration Low-Return Turbulence Pressure Tunnel	Closed Return	0.9 m x 2.29 m	120 m/s	0.02%	NASA LTPT
Instituts for Aerodynamik and Gasdynamik der Universitat Stuttgart Laminar Wind Tunnel	Open Return	0.73 m x 2.73 m (Closed)	91 m/s	0.02%	IAG Stuttgart #1
Instituts for Aerodynamic and Gasdynamik der Universitat Stuttgart 0.37 m x 0.6 m	Open Return	0.37 m x 0.6 m (Closed)	22 m/s	0.08%	IAG Stuttgart #2

and Stuttgart tunnels are low turbulence tunnels designed specifically for airfoil testing and research. Data for two airfoils, NACA 4415 and NACA 23012, are available from three of these tunnels and are presented in Figure 18-19.

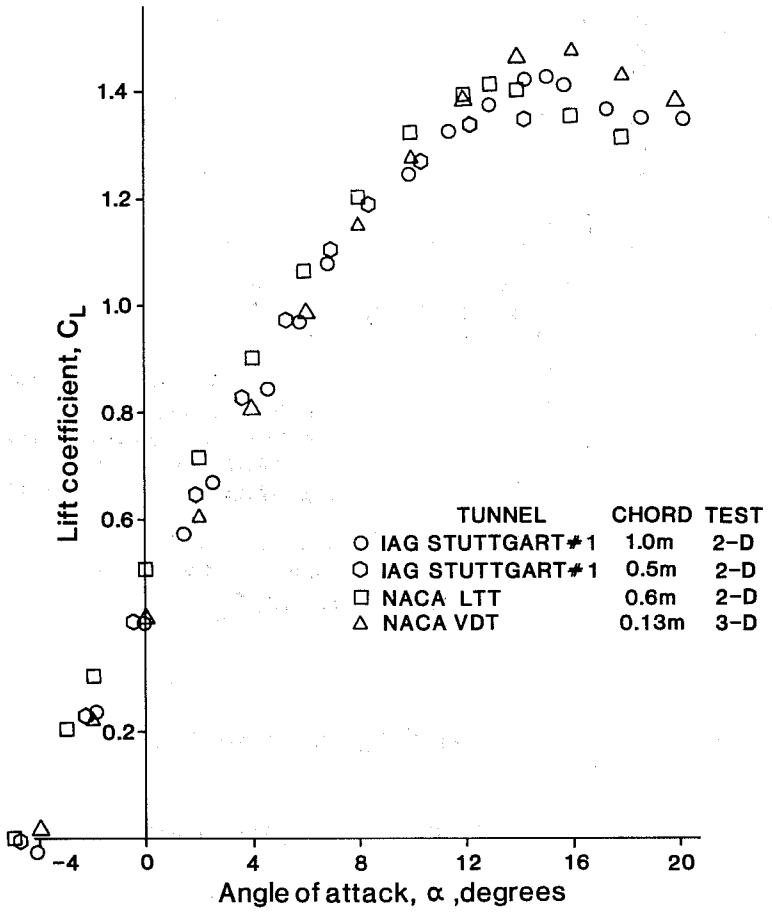

(a) Lift coefficient.

Figure 18. Comparison of airfoil data for the NACA 4415 at a Reynolds number of R_N=1.5x10^6

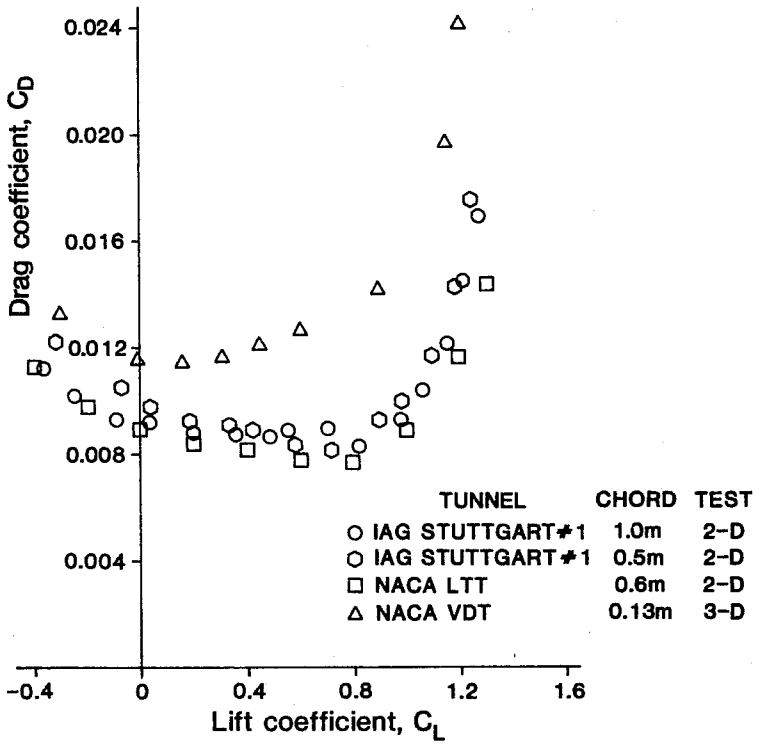

(b) Drag coefficient.

Figure 18. Concluded

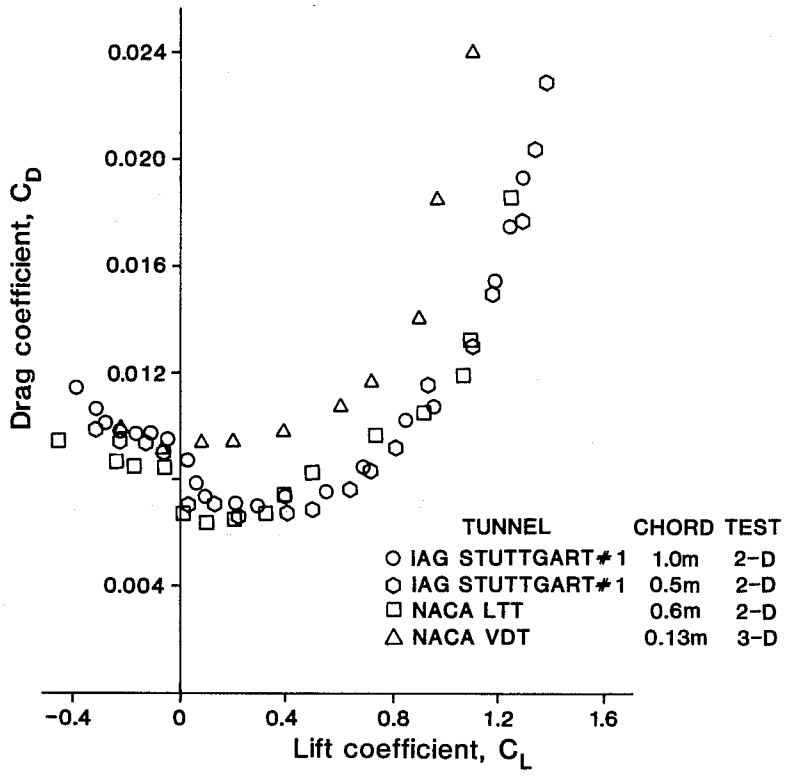

(a) Drag coefficient

Figure 19. Comparison of airfoil data for the NACA 23012 at a Reynolds number of R_N=1.5x10^6.

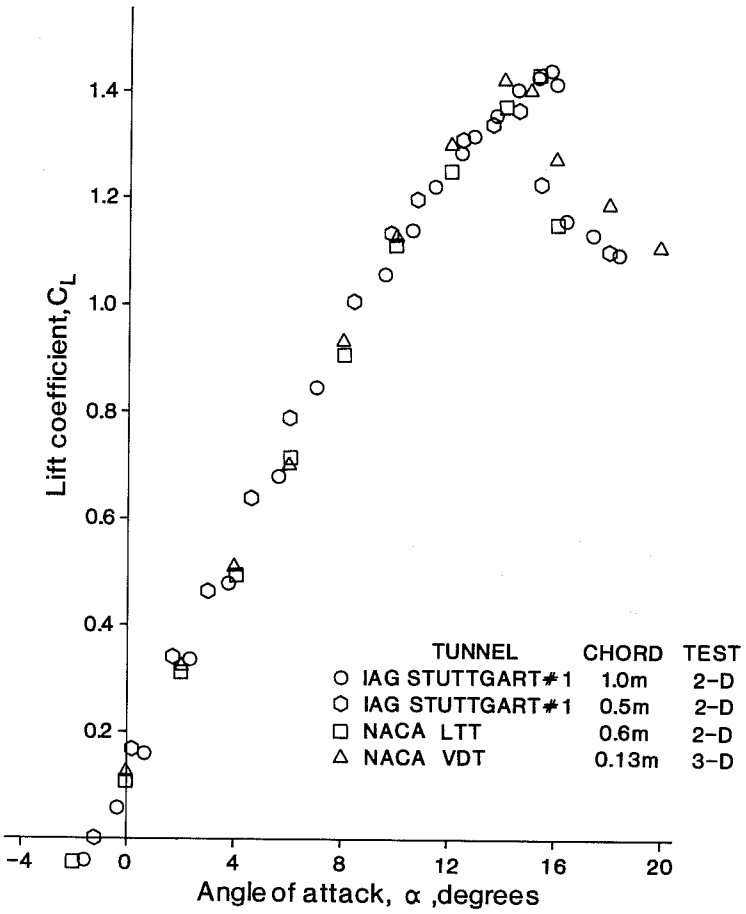

(b) Lift coefficient

Figure 19. Concluded

The test Reynolds number was 1.5×10^6. There are four sets of data, representing four separate test models with different chord lengths. Two of the models were run in the same tunnel, IAG Stuttgart #1. For lift coefficient, there is much more variation in the NACA 4415 data than in the NACA 23012 data. The same is true of the drag coefficient data, except for the NACA VDT. The high turbulence level of the NACA VDT increases the measured drag well above the other tunnels. Also, the NACA VDT data are for a three-dimensional model versus two-dimensional models for the NACA LTT and IAG Stuttgart #1 tunnels. There are no data available for comparisons with the AVA Gottingen or IAG Stuttgart #2 tunnels.

3. Airfoil Selection and Utilization of the Data

There are some essential considerations involved in the selection of an airfoil from a data catalog. First, and most important, is that there are no absolutes regarding the validity of airfoil data. There will be some variation from tunnel to tunnel, and, as seen in Figures 18-19, from test model to test model of the same airfoil in the same tunnel. There is relatively good correlation between data from the NACA LTT and IAG Stuttgart #1 tunnels. Considering also that these are two-dimensional, low turbulence tunnels, the airfoil data obtained from them should be given high credibility. This is also the case for the IAG Stuttgart #2 tunnel. Airfoil data from the AVA Gottingen and NACA VDT tunnels are affected by turbulence and the three-dimensionality of the tests. Turbulence has both positive and negative influences on the data. At low angles of attack, turbulence causes the measured drag values to be high, whereas at high angles of attack and low Reynolds numbers, turbulence works against flow separation and can cause measured drag values to be low. At low Reynolds numbers, turbulence helps achieve higher lift coefficients again by working against separation. These effects are seen in Figure 20, which compares data from the NACA VDT and NACA LTT tunnels.

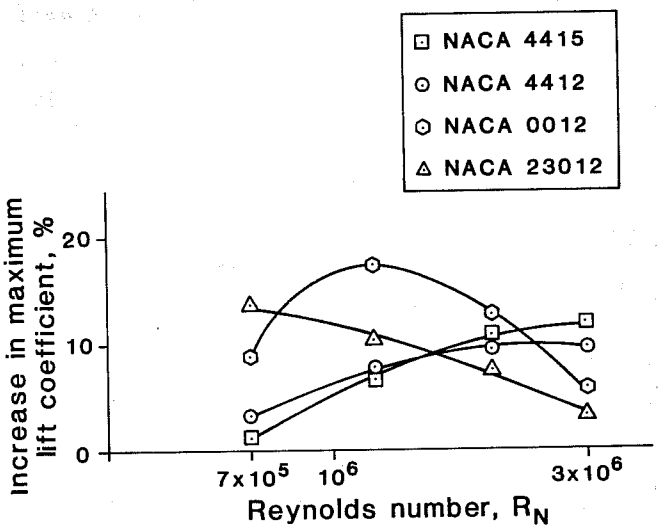

(a) Effects on maximum lift coefficient: $(C_{L_{max}})_{VDT} - (C_{L_{max}})_{LTT}$

Figure 20. Comparison of data from the NACA VDT and NACA LTT wind tunnels showing the effects of flow turbulence.

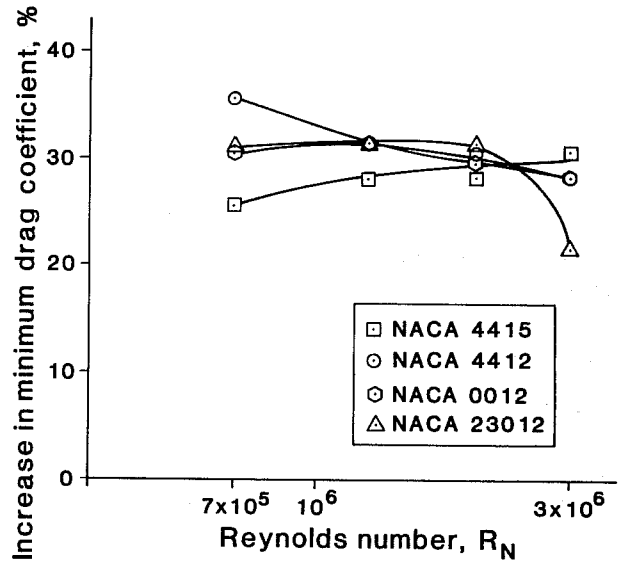

(b) Effects on minimum drag coefficient: $(C_{D_{min}})_{VDT} - (C_{D_{min}})_{LTT}$

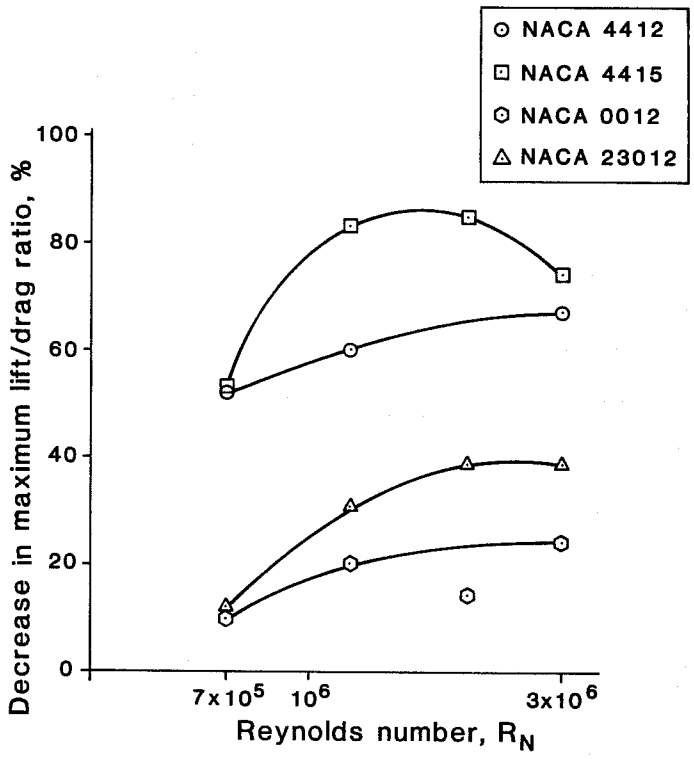

(c) Effects on maximum lift/drag ratio: $[(C_L/C_D)_{max}]_{VDT} - [(C_L/C_D)_{max}]_{LTT}$

Figure 20. Concluded

The ordinate values are percentage changes relative to the NACA LTT data. Turbulence increases the measured drag and maximum lift, and decreases the maximum lift/drag ratio. There is also the question of 3-D versus 2-D data here. In general, one should expect data from tunnels with high turbulence levels to be too high in drag, and at low Reynolds numbers, too high in maximum lift.

A second important consideration is the quality of surface of the production wing or blade including the accuracy of the airfoil contour and the smoothness of the surface material. The higher performing airfoils such as the NACA six-digit series and the Wortmann FX-series, achieve this performance through tight control of the boundary layer. The more performance a designer tries to obtain from an airfoil design, the more exacting are the requirements imposed on maintaining a particular boundary layer behavior. Exacting requirements on the boundary layer mean maintaining a highly accurate airfoil contour and a smooth surface. In short, there is a price that must be paid for increased performance beyond a certain limit. The concern here is with roughness. The high performance airfoils are especially vulnerable to surface irregularities and roughness. This has been experienced repeatedly with aircraft wings and in particular to sailplanes where aerodynamic performance is of prime importance. The question of Reynolds number influences enters here also, in that the experience with aircraft is well above SWECS in terms of Reynolds number. Data from Reference (4), which are included in this catalog, show no real advantage for surface roughness. Data for minimum drag coefficient and maximum lift coefficient are given in Figure 21.

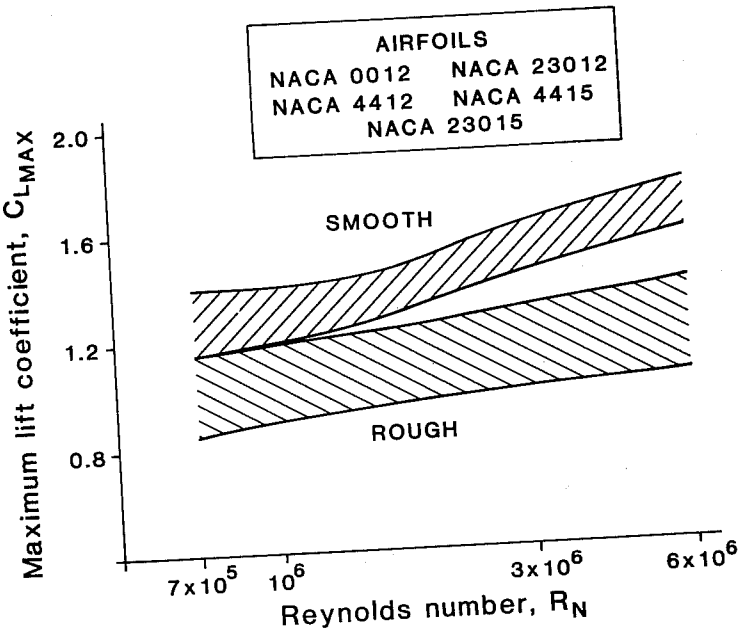

(a) Effects on maximum lift coefficient for NACA four-digit and five-digit airfoils.

Figure 21. Surface roughness effects on different NACA airfoils.

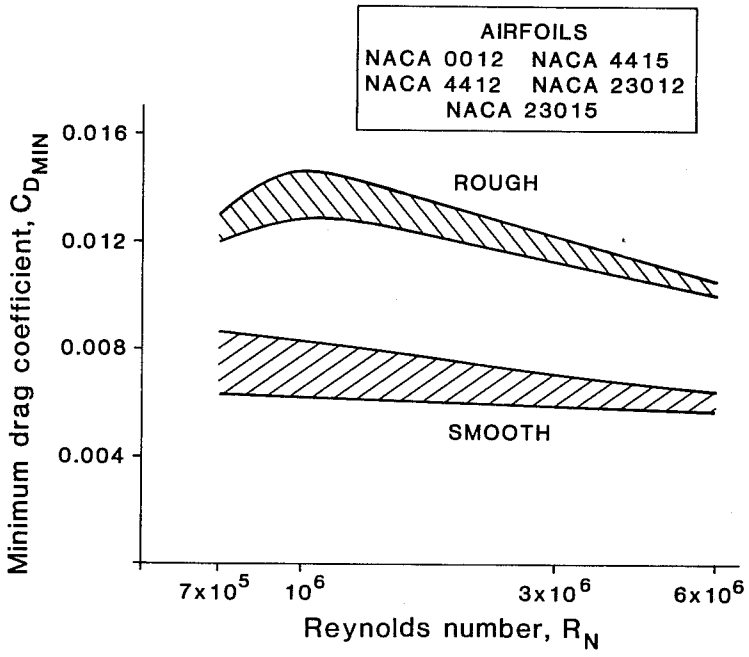

(b) Effects on minimum drag coefficient for NACA four-digit and five-digit airfoils.

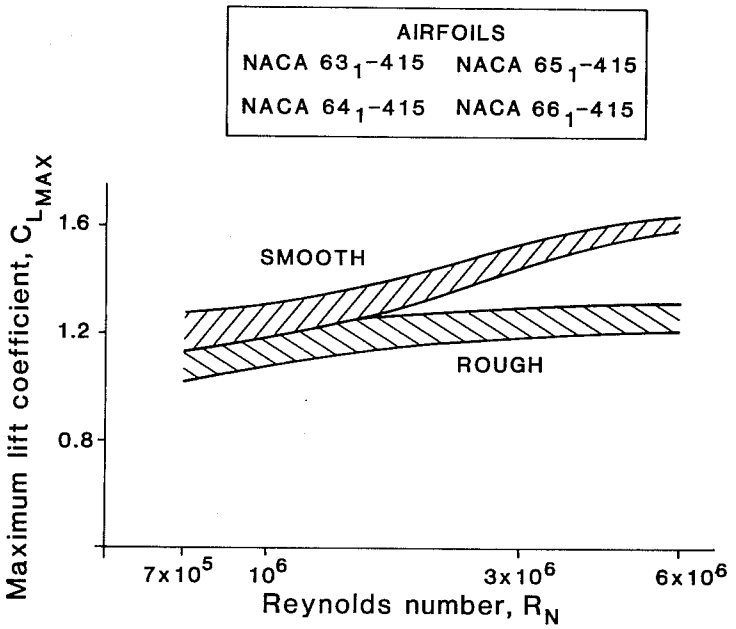

(c) Effects on maximum lift coefficient for NACA six-digit airfoils.

Figure 21. Continued

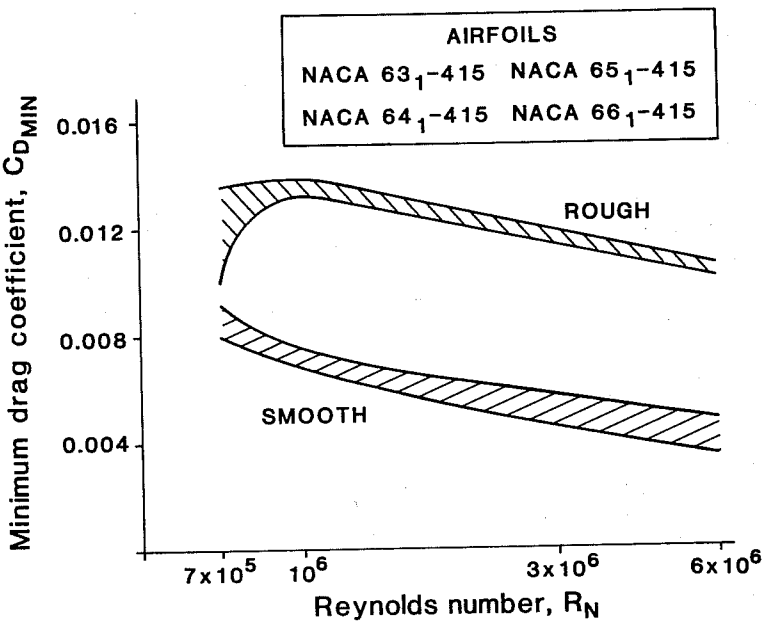

(d) Effects on minimum drag coefficient for NACA six-digit airfoils.

Figure 21. Concluded

The roughness used was 0.28 mm carborundum grains spread over the first eight percent of the airfoil at the leading edge. The data indicate that the effects of this particular roughness are reduced as the Reynolds number decreases below $R_N = 1.0 \times 10^6$. References (5) and (6), each reporting on a different high performance Wortmann FX airfoil, indicate that the respective airfoil drag values are very sensitive to surface quality.

At this point, there are no definite conclusions concerning the effect of surface quality on high performance airfoils in SWECS applications. The available evidence suggests that some caution be exercised here until additional pertinent data are available.

V. AIRFOIL DATA AT LARGE ANGLES OF ATTACK

As part of the catalog, it was originally planned to include airfoil data for angles of attack beyond stall up to ninety degrees. While there is data available, the current state of technology at the time of publication of this catalog did not allow the practical application of this data to SWECS design. There are two problem areas involved here. The first is the validity of the existing two-dimensional data. Figure 22, taken from Reference (7) shows a comparison between airfoil surface pressure measurements and force measurement of a NACA 0015.

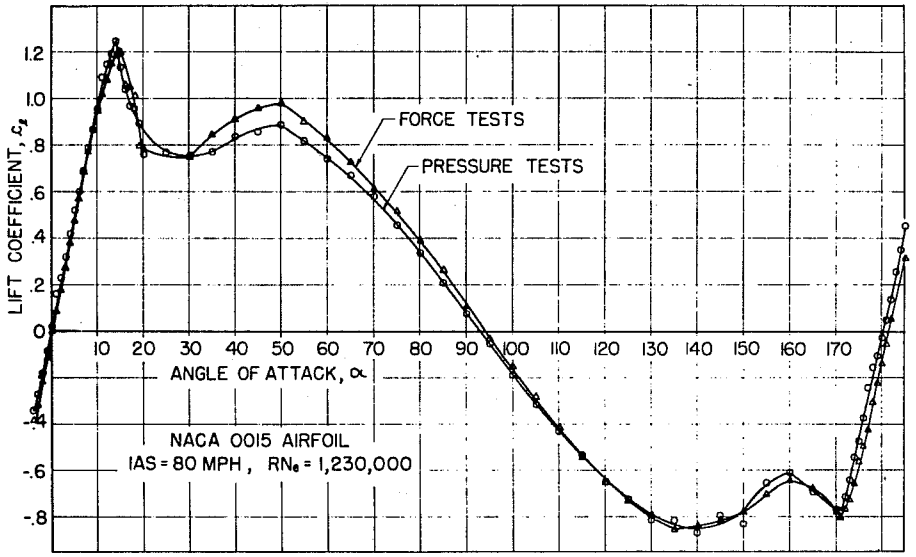

(a) Lift coefficient.

Figure 22. Comparison of force and airfoil surface pressure measurements of lift and drag coefficient for high angles of attack. Reproduced from Reference (7).

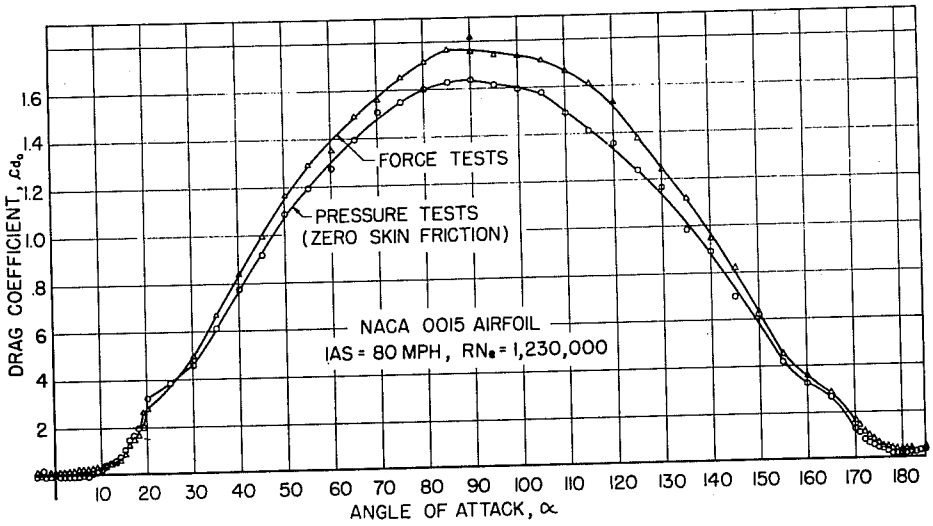

(b) Drag coefficient.

Figure 22. Concluded

Referring to Figure 17, two-dimensional testing is preferable for airfoil measurements because the presence of the test section walls have minimal effect on the test model for normal angles of attack ($\alpha<20^{o}$). The separated flow pattern is affected by the presence of the walls and a different behavior is obtained on the test model in the middle of the test section than near the walls. Force measurements cannot detect this, and provide only the resultant model force due to the combined separated flow pattern. If force measurements are to be made, then only the center section of the model should be connected to the force balance. This poses mechanical problems. More reliable results can be obtained with surface pressure measurements on the model in the center of the test section. Most of the two-dimensional airfoil data available, however, came from force measurements and are thus open to question.

The second problem area is the conversion of the two-dimension data to the actual three-dimensional wing. Unlike the unstalled, low angle of attack case where the two-dimensional flow over the airfoil is similar to that over the wing, the stalled, separated flows are different. This can be seen in Figure 23, reproduced from Reference (8).

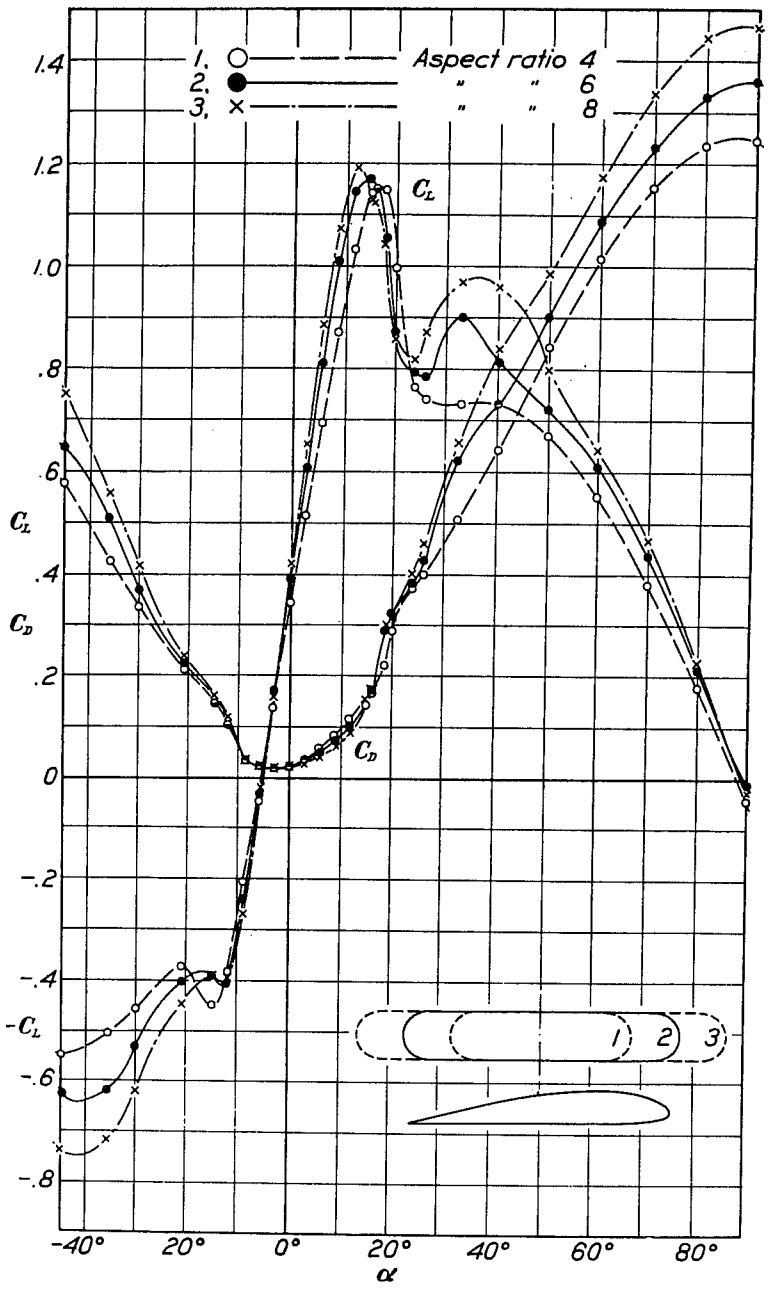

Figure 23. Effect of aspect ratio on the aerodynamic behavior of a wing at high angles of attack. Clark Y airfoil. Reproduced from Reference (8).

Conversion of stalled airfoil data to the wing or wind turbine blade requires an empirically developed relation which is as yet unknown to the author. An attempt was made to construct such a relation using the flat plate model formulated by Norton (9). This model predicts the lift and drag coefficients of a flat plate for angles of attack ($\alpha > 20^\circ$) and for arbitrary aspect ratios. Because of its thin leading edge, the flat plate stalls sooner, and has correspondingly lower lift and higher drag then conventional airfoils. The author believes, however, that this model could be made to work with some empirical adjustment to account for the thick, rounded leading edge of airfoils. Figure 24, also taken from Reference (8) shows that wing or blade tip shape has no appreciable effect.

The post-stall peak lift and drag coefficients increase toward their respective two-dimensional values as the aspect ratio increases (= ∞ for two-dimensional). The difference in airfoil sections between Figures 22 and 23 has significance only in that the corresponding two-dimensional values of the Clark-Y in Figure 23 would be expected to be slightly different than those of the NACA 0015 of Figure 22.

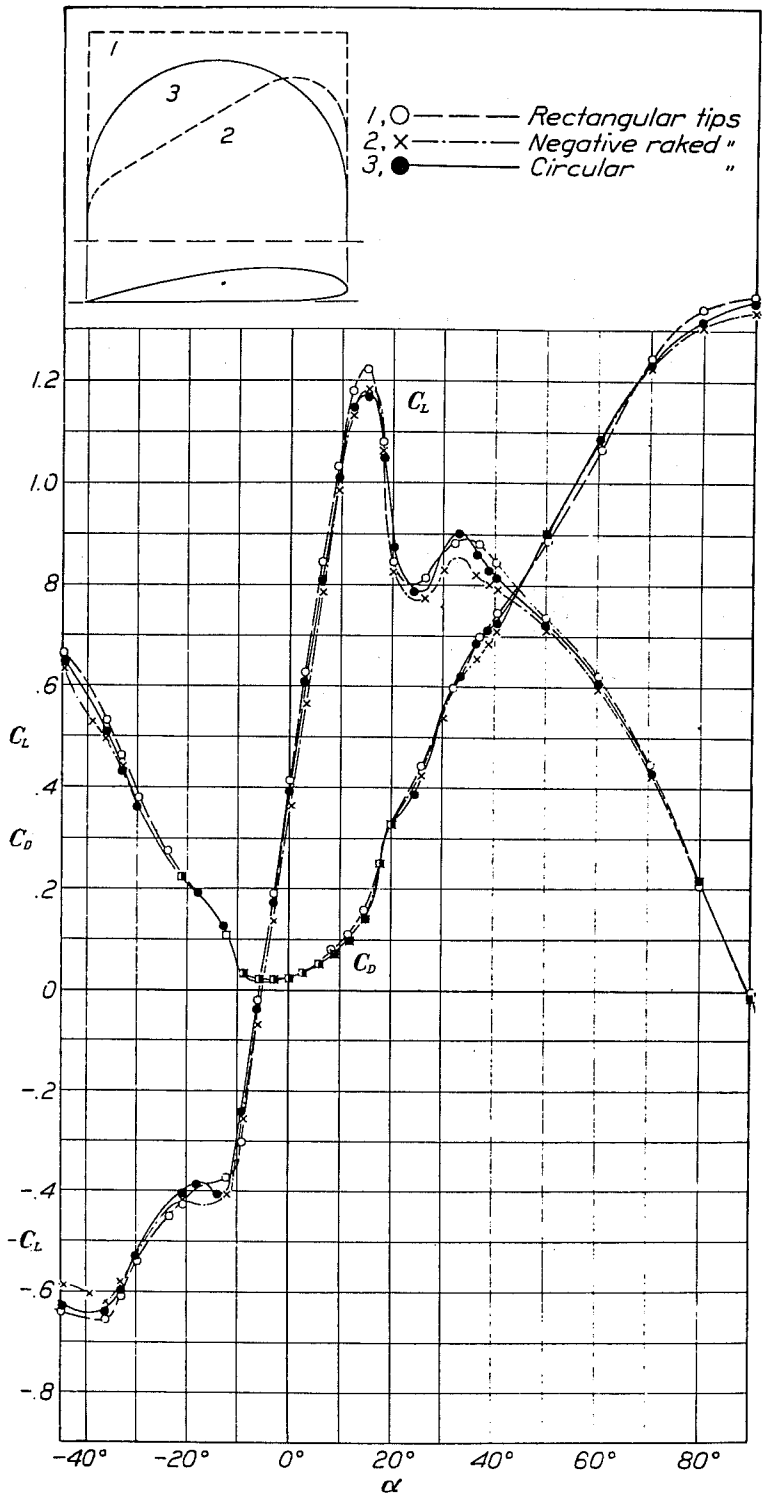

Figure 24. Effect of tip shape on the aerodynamic behavior of a wing at high angles of attack. Reproduced from Reference (8).

VI. AIRFOIL DATA

The airfoil data presented in the catalog are organized as follows: first page: airfoil section designation, test conditions and profile contour; second page: airfoil section coordinates; third page: graphical presentation of airfoil characteristics including lift coefficient, drag coefficient, pitching moment coefficient at the quarter-chord and lift/drag ratio; fourth page: tabulation of the coefficient values as a function of angle of attack (AOA) and Reynolds number. If more pages are required for the data, the third- and/or fourth-page formats are repeated.

The data values presented were obtained in the following manner. The original airfoil data were in graphical form as presented in the respective reports and papers. Data values were taken from each curve using a digitizing procedure. The graph was placed on a digitizing board which was connected to a microcomputer. An airfoil digitizing program code was formulated to operate the system. Four reference points were selected for each graph coordinate system to develop a coordinate transformation. This was done to compensate for any distortion that may have been introduced into the original as a result of reproduction. The digitized data were stored on floppy disk for additional processing. The tabulated values were obtained from the digitized values using a standard cubic spline interpolation procedure. As part of the processing, the drag coefficients were converted from dependency on lift coefficient to dependency on angle of attack to facilitate use of the tabulated values for SWECS performance analyses. This was done as part of the interpolation of the lift coefficient data. The interpolation procedures used for the drag curves required considerable effort. The steep slopes at the ends of the drag curves caused numerical instabilities which resulted in large gyrations in the interpolated curve between the original data points. A coordinate transformation using the reciprocal of the log of the drag coefficient was ultimately found to work satisfactorily.

The accuracy of the tabulated values is considered to be superior to that which would be normally attained by reading the values directly from the respective curves using a scale. The digitizer board resolution was 0.01 inch in both x- and y-coordinate directions. An electronic cross hair incorporated into a magnifying lens establishes the point to be digitized. Correct evaluation and scaling of the coordinate pair is done by the processing program which removes human error from the procedure. The end result is that the curves were read as accurately as practical, considering their basic accuracy as a data presentation form.

The graphical data presented on the third pages of the data sequence were subjected to an additional numerical smoothing procedure to "clean up"

the curves' appearance. These data may consequently show some small differences from the tabulated values. The graphical data are presented only to provide a qualitative indication of the respective airfoil's performance.

An index of the airfoils contained in the catalog is provided in Table A-I.

VII. REFERENCES

1. Abbott, I.H. and von Doenhoff, A.E., Theory of Wing Sections, Dover Publications, Inc., New York, 1959.

2. Miley, S.J., An Analysis of the Design of Airfoil Sections for Low Reynolds Numbers, Ph.D. Dissertation, Mississippi State University, 1972.

3. Kraemer, K., Windkanalmessungen am Profil Go 769, AVA Gottingen Report 57/A/25, 1957.

4. Loftin, L.K., Jr. and Smith, H.A., Aerodynamic Characteristics of 15 NACA Airfoil Sections at Seven Reynolds Numbers from 0.7 x 10^6 to 9.0 x 10^6, NACA Technical Note 1945, October, 1949.

5. Gooden, J.H.M., "Experimental Low-Speed Aerodynamic Characteristics of the Wortmann FX 66-S-196 VI Airfoil," Presented at the XVI OSTIV Congress, Chateauroux, France, 1978.

6. Somers, D.M. and Foster, J.M., An Exploratory Investigation of the Effects of a Plastic Coating on the Profile Drag of a Practical-Metal-Construction Sailplane Airfoil, NASA Technical Memorandum 80092, July, 1979.

7. Pope, A., "The Forces and Pressures over an NACA 0015 Airfoil Through 180 Degrees Angle of Attack," Aero Digest, Vol 58, No. 4, April, 1949.

8. Knight, M. and Wenzinger, C.J., Wind Tunnel Tests on a Series of Wing Models Through a Large Angle of Attack Range, Part 1, Force Tests, NACA Report 317, 1929.

9. Norton, D.J. and Chevalier, H.L., Wind Loads on Solar Collector Panels and Support Structure, Aerospace Engineering Department, Texas A&M University, October, 1979.

NACA 66(2)–415

NACA 66(2)-415
Reference: (A3)
Wind Tunnel: NACA LTT
Date: 1945
Type of Test: Two-Dimensional
Wind Tunnel Turbulence: 0.03%
Airfoil Surface: Smooth
Reynolds Number: $7.0 \times 10^5 - 3.0 \times 10^6$

Airfoil Surface: Rough
Reynolds Number: $7.0 \times 10^5 - 2.0 \times 10^6$

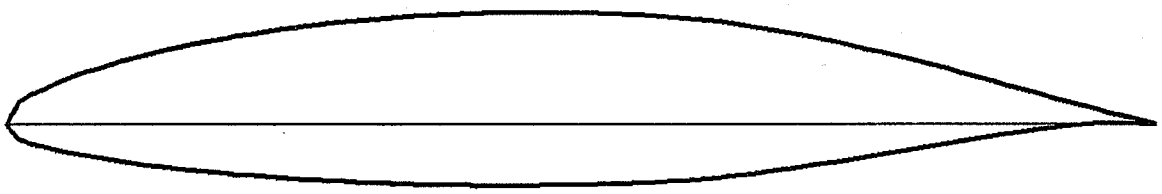

NACA 66(2)-415 X,Y Coordinates

X(upper)	Y(upper)	X(lower)	Y(lower)
.00000	.00000	.00000	.00000
.00314	.01206	.00686	-.01006
.00544	.01467	.00956	-.01187
.01019	.01873	.01481	-.01445
.02241	.02592	.02759	-.01848
.04711	.03718	.05289	-.02454
.07199	.04617	.07801	-.02921
.09696	.05381	.10304	-.03313
.14709	.06624	.15291	-.03932
.19736	.07581	.20264	-.04397
.24771	.08329	.25229	-.04749
.29812	.08897	.30188	-.05009
.34857	.09309	.35143	-.05189
.39904	.09571	.40096	-.05287
.44952	.09685	.45048	-.05305
.50000	.09656	.50000	-.05244
.55046	.09473	.54954	-.05093
.60090	.09100	.59910	-.04816
.65126	.08431	.64874	-.04311
.70150	.07518	.69850	-.03630
.75162	.06419	.74838	-.02839
.80159	.05187	.79841	-.02003
.85139	.03872	.84861	-.01180
.90104	.02519	.89896	-.00451
.95053	.01196	.94947	.00068
1.00000	.00000	1.00000	.00000

leading edge radius = 1.435
slope of radius = 0.168

NACA 66(2)–415

Reynolds Number		Test Conditions	
7.0×10^5	———	Tunnel:	NACA LTT
1.0×10^6	·····	Date:	1945
1.5×10^6	·····	Test:	2–D
2.0×10^6	·····	Turbulence:	0.03%
3.0×10^6	·····	Surface:	Smooth

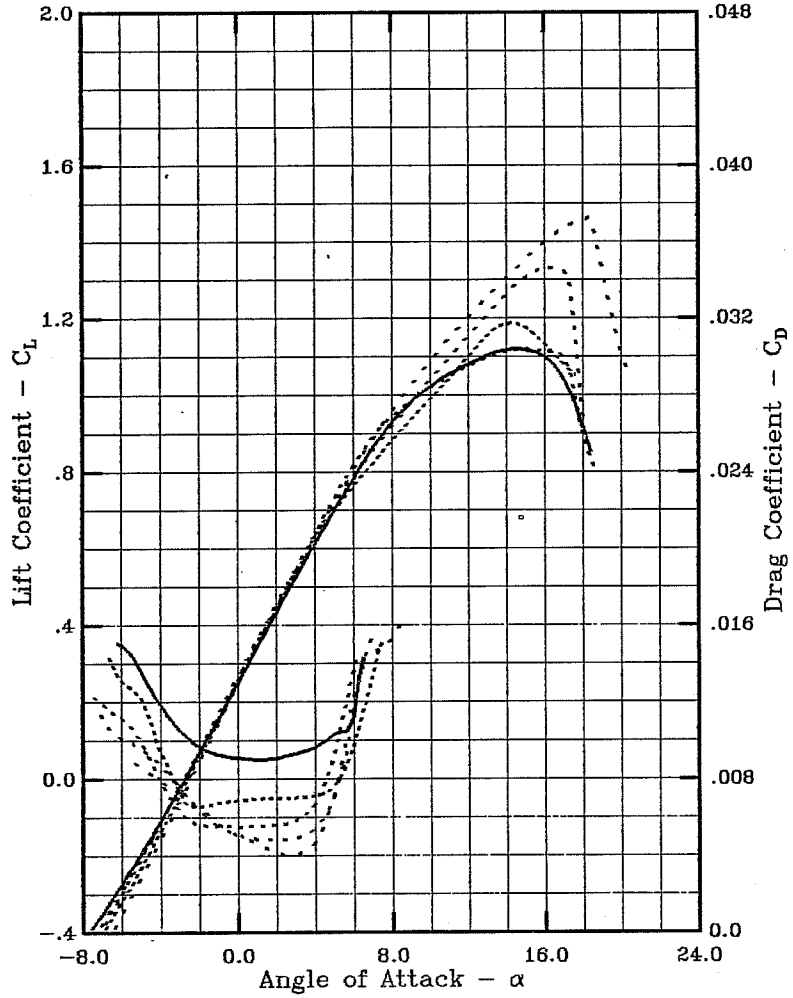

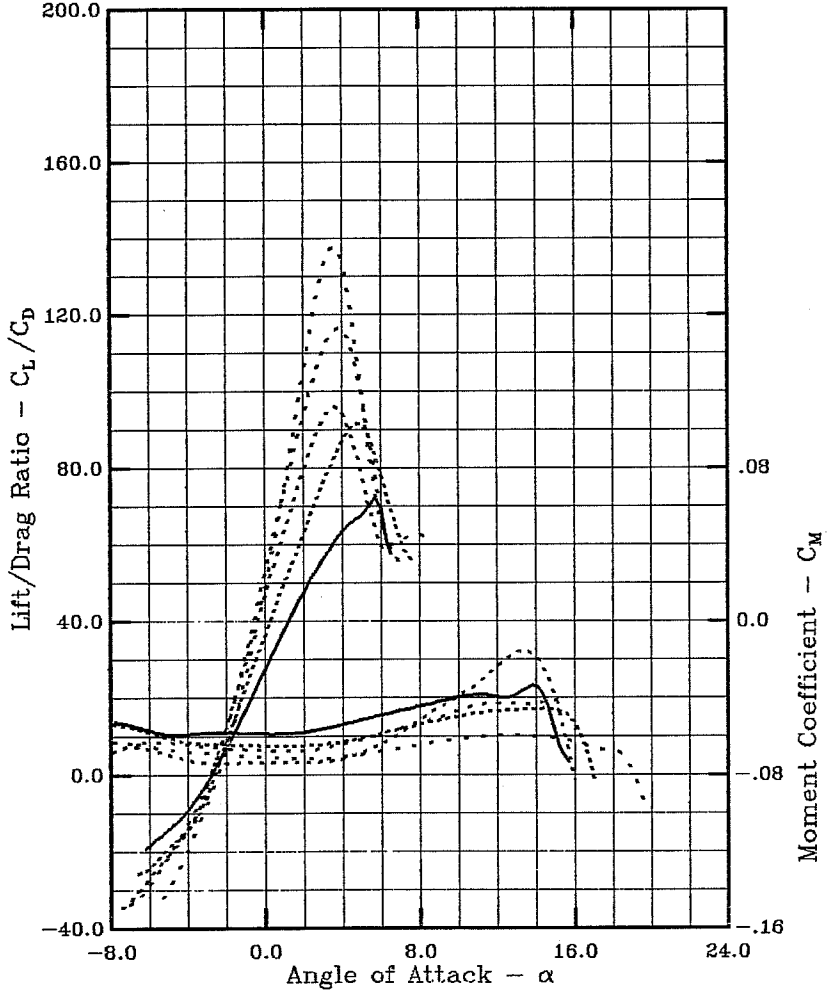

NACA 66(2)-415

Tunnel: NACA LTT / Date: 1945 / Test: 2-D / Turbulence: 0.03% / Surface: Smooth

RN	7.0×10^5			1.0×10^6			1.5×10^6			2.0×10^6			3.0×10^6		
AOA	CL	CD	CM	CL	CD	CM	CL	CD	CM	CL	CD	CM	CL	CD	CM
-8.0	-.42	-	-.05	-.48	-	-.05	-	-	-.07	-.46	-	-.06	-	-	-
-7.0	-.35	-	-.05	-.40	-	-.06	-.39	.0119	-.07	-.38	.0112	-.06	-	-	-.06
-6.0	-.28	.0149	-.06	-.32	.0131	-.06	-.30	.0111	-.07	-.29	.0101	-.06	-.35	-	-.07
-5.0	-.19	.0136	-.06	-.23	.0121	-.06	-.21	.0099	-.07	-.20	.0096	-.06	-.25	.0086	-.07
-4.0	-.11	.0118	-.06	-.14	.0095	-.06	-.11	.0079	-.07	-.11	.0087	-.06	-.15	.0079	-.07
-3.0	-.02	.0105	-.06	-.04	.0073	-.06	-.02	.0063	-.07	-.02	.0076	-.07	-.05	.0072	-.07
-2.0	.07	.0097	-.06	.06	.0065	-.06	.07	.0056	-.07	.08	.0064	-.07	.05	.0065	-.07
-1.0	.16	.0093	-.06	.15	.0067	-.06	.16	.0055	-.07	.17	.0056	-.07	.15	.0057	-.07
.0	.25	.0091	-.06	.25	.0069	-.06	.26	.0055	-.07	.27	.0051	-.07	.25	.0051	-.07
1.0	.34	.0090	-.06	.35	.0070	-.06	.35	.0055	-.07	.36	.0049	-.07	.34	.0046	-.07
2.0	.43	.0091	-.06	.44	.0070	-.06	.44	.0056	-.07	.45	.0048	-.07	.44	.0042	-.07
3.0	.52	.0093	-.06	.53	.0070	-.06	.54	.0058	-.07	.54	.0049	-.07	.54	.0041	-.07
4.0	.61	.0096	-.05	.62	.0071	-.06	.64	.0067	-.07	.63	.0054	-.06	.63	.0047	-.07
5.0	.70	.0103	-.05	.70	.0076	-.06	.73	.0093	-.07	.71	.0072	-.06	.72	.0072	-.07
6.0	.78	.0114	-.05	.76	.0097	-.06	.82	.0137	-.06	.79	.0116	-.06	.80	.0122	-.07
7.0	.86	-	-.05	.82	.0135	-.06	.89	-	-.06	.86	-	-.06	.88	.0146	-.07
8.0	.93	-	-.04	.88	-	-.05	.94	-	-.05	.92	-	-.05	.96	.0153	-.06
9.0	.98	-	-.04	.94	-	-.05	.99	-	-.05	.98	-	-.05	1.03	-	-.06
10.0	1.02	-	-.04	.99	-	-.05	1.02	-	-.04	1.04	-	-.05	1.09	-	-.06
11.0	1.05	-	-.04	1.04	-	-.05	1.05	-	-.03	1.10	-	-.04	1.15	-	-.06
12.0	1.08	-	-.04	1.10	-	-.05	1.08	-	-.02	1.15	-	-.04	1.20	-	-.06
13.0	1.10	-	-.04	1.15	-	-.05	1.10	-	-.02	1.21	-	-.04	1.25	-	-.06
14.0	1.12	-	-.03	1.18	-	-.05	1.11	-	-.02	1.26	-	-.04	1.30	-	-.06
15.0	1.12	-	-.06	1.18	-	-.05	1.12	-	-.04	1.31	-	-.04	1.35	-	-.06
16.0	1.10	-	-	1.13	-	-.05	1.11	-	-.08	1.33	-	-	1.40	-	-.06
17.0	1.04	-	-	1.08	-	-.08	1.10	-	-	1.32	-	-	1.44	-	-.07
18.0	0.92	-	-	-	-	-	0.90	-	-	0.95	-	-	1.46	-	-.07
19.0	-	-	-	-	-	-	-	-	-	-	-	-	1.33	-	-.08
20.0	-	-	-	-	-	-	-	-	-	-	-	-	1.11	-	-

NACA 66(2)–415

Reynolds Number		Test Conditions	
7.0×10^5	———	Tunnel:	NACA LTT
1.0×10^6	·····	Date:	1945
1.5×10^6	·····	Test:	2–D
2.0×10^6	·····	Turbulence:	0.03%
		Surface:	Rough

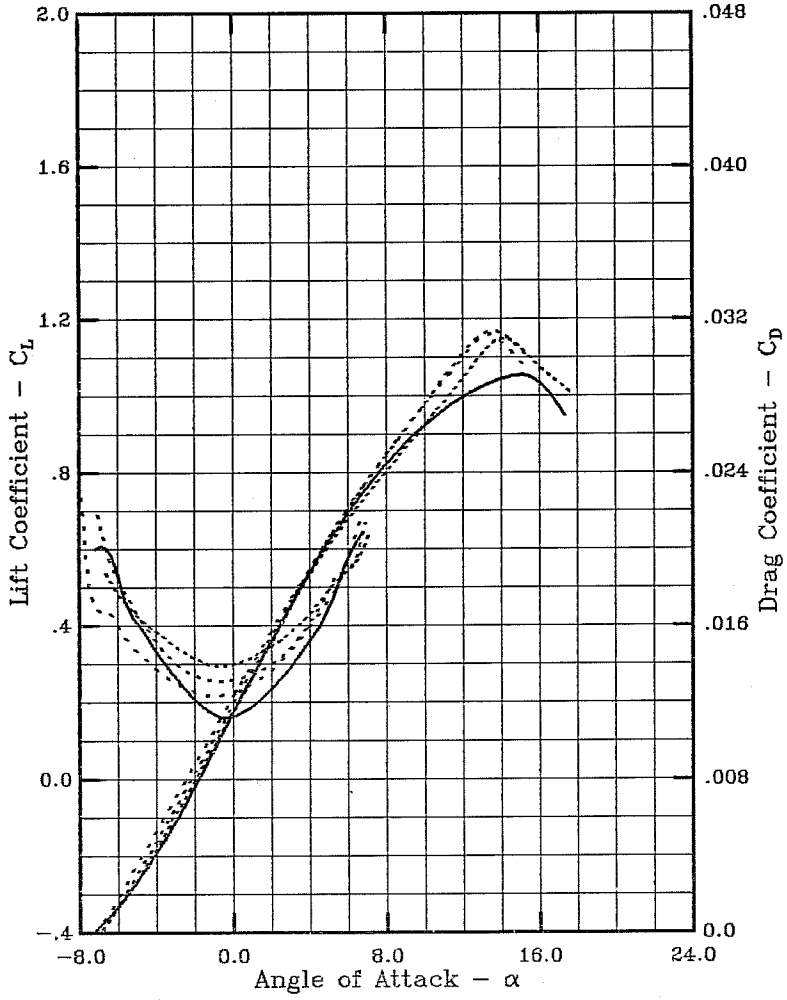

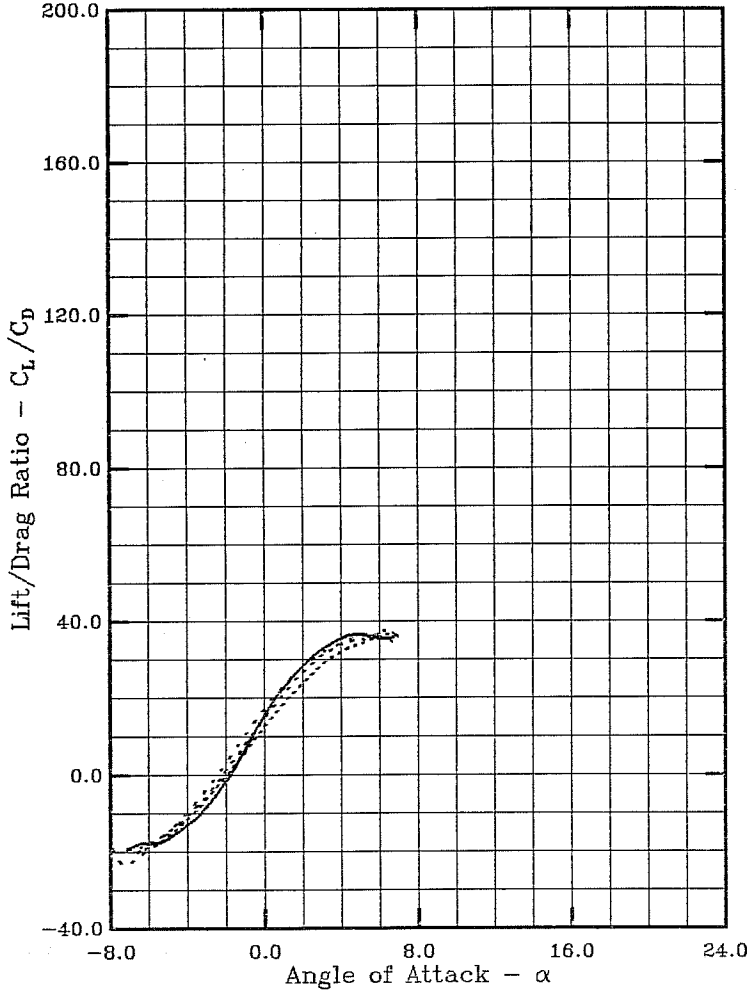

NACA 66(2)-415

Tunnel: NACA LTT / Date: 1945 / Test: 2-D / Turbulence: 0.03% / Surface: Rough

RN	7.0×10^5		1.0×10^6		1.5×10^6		2.0×10^6	
AOA	CL	CD	CL	CD	CL	CD	CL	CD
-8.0	-	-	-.46	-	-.48	-	-.43	.0235
-7.0	-.38	.0201	-.40	-	-.41	.0215	-.39	.0168
-6.0	-.33	.0187	-.33	.0177	-.33	.0185	-.31	.0160
-5.0	-.27	.0162	-.26	.0165	-.25	.0166	-.22	.0147
-4.0	-.19	.0147	-.18	.0157	-.16	.0152	-.13	.0137
-3.0	-.11	.0133	-.09	.0149	-.07	.0141	-.05	.0130
-2.0	-.02	.0122	-.00	.0143	.02	.0134	.04	.0125
-1.0	.08	.0114	.09	.0139	.10	.0131	.13	.0123
.0	.17	.0113	.18	.0140	.19	.0132	.21	.0125
1.0	.27	.0118	.27	.0144	.28	.0134	.30	.0130
2.0	.36	.0127	.36	.0149	.37	.0140	.38	.0137
3.0	.45	.0138	.45	.0157	.46	.0148	.47	.0147
4.0	.54	.0152	.53	.0166	.55	.0161	.55	.0160
5.0	.62	.0169	.61	.0178	.63	.0179	.63	.0173
6.0	.69	.0195	.68	.0188	.70	.0190	.71	.0194
7.0	.76	-	.74	.0206	.78	.0218	.78	-
8.0	.82	-	.80	-	.84	-	.85	-
9.0	.88	-	.86	-	.91	-	.91	-
10.0	.92	-	.92	-	.98	-	.98	-
11.0	.96	-	.98	-	1.05	-	1.04	-
12.0	1.00	-	1.04	-	1.11	-	1.10	-
13.0	1.02	-	1.11	-	1.16	-	1.15	-
14.0	1.04	-	1.15	-	1.16	-	1.14	-
15.0	1.05	-	1.13	-	1.12	-	1.09	-
16.0	1.03	-	1.07	-	-	-	-	-
17.0	.98	-	1.03	-	-	-	-	-